Vibronic recovering of functionality of quantum cellular automata based on bi-dimeric square cells with violated condition of strong Coulomb repulsion

Boris Tsukerblat,*[1,3] Andrew Palii,*[2] Shmuel Zilberg,[3] Denis Korchagin,[2]
Sergey Aldoshin,[2] Juan Modesto Clemente-Juan[5]

[1]*Ben-Gurion University of the Negev, Beer-Sheva, Israel*
[2]*Institute of Problems of Chemical Physics of RAS, Chernogolovka, RF*
[3]*Department of Chemical Sciences, Materials Research Center, Ariel University, Ariel, Israel*
[4]*Instituto de Ciencia Molecular, Universidad de Valencia, Paterna, Spain*

* *Corresponding authors' e-mails*: tsuker@bgu.ac.il (B.T.); andrew.palii@uv.es (A.P.)

Abstract

Strong Coulomb repulsion between the two charges in a square planar mixed-valence cell in quantum cellular automata (QCA) allows to encode the binary information in the two energetically beneficial diagonal distributions of the electronic density. In this article we pose a question: to what extent is this condition obligatory for the design of the molecular cell? To answer this question, we examine the ability to use square-planar cell composed of one-electron mixed valence dimers to function in QCA in a general case when the intracell Coulomb interaction *U* is not supposed to be extremely strong, which means that it is comparable with the characteristic electron transfer energy (violated strong *U* limit). Using the two-mode vibronic model treated within the semiclassical (adiabatic) and quantum-mechanical approaches we demonstrate that strong vibronic coupling is able to create a considerable barrier between the two diagonal-type charge configurations thus ensuring bistability and polarizability of the cells even if the Coulomb barrier is not sufficient. The cases of weak and moderate Coulomb repulsion and strong vibronic coupling are exemplified by consideration of the cation-radicals of the two polycyclic derivatives of norbornadiene $[C_{12}H_{12}]^+$ and $[C_{17}H_{16}]^+$ with the terminal C=C chromophores playing the role of redox sites. By using the detailed *ab initio* data we reveal the main characteristics of the bidimeric cells composed of these molecules and illustrate the pronounced effect of the vibronic recovery clearly manifesting itself in the shape of the cell-cell response function. Revealing of such "vibronic recovery" of strong localization when the strong *U* limit is violated suggests a way to a significant expansion of the class of molecular systems suitable as QCA cells.

1.Introduction

The idea of molecular quantum cellular automat (MQCA) [1-8] represents continuation and further development of the initial idea to use quantum dots as building blocks of quantum cellular automata (QCA). It suggests to use organic mixed-valence (MV) molecules and transition metal MV clusters for the creation of QCA cells [9-14]. Basically, the QCA cell consists of four redox centers forming a square and two excess electrons or holes enabling to encode binary information in stable charge configurations. The Coulomb repulsion between the two charges favors two bistable diagonal-type charge configurations allowing to encode logic "0" and "1". The binary information is transmitted from cell to cell via the intercell Coulomb interaction. The presence of the electron transfer between the redox centers in MV molecules usually occurring through the bridging ligands makes it possible to produce switching between the diagonal charge configurations.

MQCA have distinct advantages over QCA based on quantum dots such as much higher functional device density and also much higher speed of QCA operations. The latter is due to the fact that electron transfer in MV clusters typically occurs at a picosecond timescale [15]. Implementation of QCA approach at a molecular scale has stimulated much efforts in chemistry and molecular electronics, including synthesis and experimental characterization of suitable MV molecular candidates [16-27] as well as theoretical studies of different aspects of their functioning including *ab initio* quantum chemical calculations [3-6, 28-31], elaboration of parametric theoretical models [32-43], and the analysis of power dissipation accompanying the switching process [44].

Up to now in most studies dealing with theoretical modelling of four-dot two-electron square cells the Coulomb repulsion between the electrons has been assumed to be a dominating electronic interaction within the cell in the sense that Coulomb energy gap U separating energetically favorable charge configurations (electronic pair occupies diagonal positions) from the excited configurations (sides of the square occupied by two electrons) considerably exceeds the electron transfer energy t, that is the inequality $U>>t$ is implied. Just in this case an appreciable Coulomb barrier separating two distinct diagonal-type charge configurations appears enabling to encode binary information. Under this condition the cell proves to be sensitive (polarizable) to the action of the field induced by the neighboring polarized driver-cell which is the necessary prerequisite for the efficient transmission of the information between the cells forming MQCA devices. In other words, it seems quite reasonable to assume that a strong Coulomb repulsion (abbreviated here as "strong U limit") is required to ensure bi-stability and polarizability of the cell and hence the proper functioning of MQCA.

In spite of the above arguments about requirement of the strong U for the cell functionality, recently we have demonstrated that this statement is only of limited validity because it ignores the interaction of MV cells with the molecular vibrations i.e. vibronic coupling. Meantime, the vibronic coupling is an inherent part of the problem of mixed-valency [45-64], and particularly this interaction has been shown

to produce strong impact on MQCA functioning [32-41, 43]. Indeed, at strong vibronic coupling, the electronic mobility proves to be strongly reduced thus facilitating polarization of the cell caused by the intercell Coulomb interaction. By analyzing the properties of square- planar cell represented by tetrameric MV transition metal cluster of d^1- d^1-d^0-d^0-type with the aid of the model including the vibronic interaction we have recently demonstrated that at strong vibronic coupling such cell can function properly even if strong *U* limit is violated [43]. This result has been explained by similarity of the effects produced by Coulomb and vibronic interactions on the localization-delocalization behavior of the electronic pair. Indeed, both these interactions tend to suppress the electron delocalization ensuring thus bi-stability and high polarizability of the cell.

In this article we extend the study of the vibronic effects in the cells with violated strong *U* limit to another kind of four-dot two-electron square cell, which represents the *A*-*B*-*C*-*D* square composed of two identical molecular dimeric half-cells *A*-*B* and *D*-*C* (Fig. 1). Each such half-cell is represented by a MV dimer with one excess electron hopping over two diamagnetic sites (e. g. d^1-d^0-dimer in the case of transition metal cluster or similar organic MV dimers). Such bi-dimeric cell can be regarded as alternative of the square cell based on MV tetramer d^1- d^1-d^0-d^0 whose ability to act as MQCA cell under violation of strong *U* limit has been analyzed in [43]. One can expect that strong vibronic coupling would be able to restore the functionality of the bi-dimeric cell broken down by the violation of the strong *U* limit as in the case of tetrameric cell. A specific feature of the bi-dimeric cells is the existence of two kinds of their mutual dispositions for which the two neighboring cells are arranged "head-to-tail" and "side-by-side". This difference will be examined below. While composing different QCA devices from such cells both these connection types are unavoidable present and this is obviously an obstacle to create functioning device in which all pairs of cells should be fully equivalent from the point of view of the intercell Coulomb interaction. Due to such specific feature of the bi-dimeric cells the main findings related to the role of vibronic coupling in the tetrameric cells [43] do not admit direct extension to the case of bi-dimeric cells, and so the vibronic problem of bi-dimeric cells requires special consideration.

Here we report the analysis of the vibronic effects in isolated and interacting square-planar bi-dimeric QCA cells in which the strong *U* limit is violated with the special emphasis on the mentioned inequivalence between head-to-tail and side-by-side types of cells connections.

2. The model

The main interactions involved in the model of QCA based on the bi-dimeric two-electron square cells are the following: 1) one-electron transfer of the excess electron which occurs within each dimeric subunit. A selected transfer process within the dimer *A*-*B* from the occupied site *A* to the empty site *B* is shown in Fig.1 As the result the electronic configuration (*A*, *C*) in which the two electrons occupy a diagonal position in the cell is transformed into the electronic configuration (*B*, *C*) with electrons

occupying the side of the square. The electron transfer parameter *t* describing such process has the same sense that the electron hopping integral in the Hubbard model. 2) the intracell Coulomb repulsion between the two excess electrons. There are two different intracell Coulomb energies corresponding to far spaced (along the diagonals) or closely spaced (along the sides) positions within the cell. The side-type electronic configurations are higher in Coulomb energy that the diagonal-type ones, the

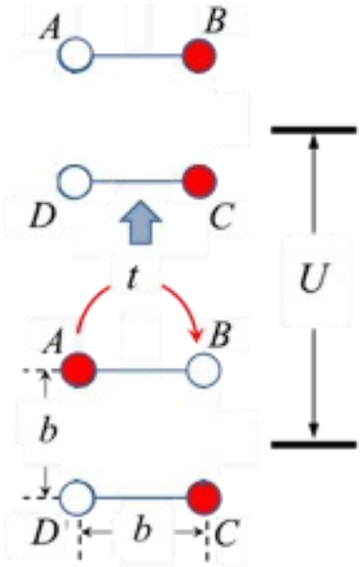

Fig. 1. Illustration for the basic electronic interactions in a bi-dimeric square cell consisting of two one-electron mixed valence dimers *A*-*B* и *D*-*C*. Each one-electron hopping process described by the transfer parameter *t* changes the Coulomb energy of the electronic pair. The excited charge configurations (electronic distributions) with closely spaced electrons are separated from ground diagonal configurations by the Coulomb energy gap *U*. The site occupied by excess electron is shown in red, and the empty site in white.

corresponding Coulomb energy gap is denoted as *U* (Fig. 1). One can see that each one-electron transfer event changes the Coulomb energy of the cell by *U*. Thus, for example, the $A \rightarrow B$ electron transfer process transforms the ground diagonal-type configuration (*A*, *C*) into the excited side-type configuration (*B*, *C*) as shown in Fig. 1. 3) vibronic interaction that will be introduced later on.

Because the electron transfer between the one-electron dimeric half-cells is forbidden according to the very sense of the bi-dimeric cell, there are only four allowed distributions of the electronic pair within the bi-dimeric cell *A*-*B*-*C*-*D*, namely, the diagonal-type distributions (*A,C*) and (*B,D*) in which the electrons occupy the far-spaced positions, and the distributions (*A*,*D*) and (*B,C*) with two closely spaced electrons belonging to different dimeric half-cells. This distinguishes the bi-dimeric cell from the tetrameric cell, in which there are six possible electronic distributions [43].

The binary information in QCA devices is transmitted from cell to cell through the intercell Coulomb repulsion. Such transmission is usually described as a response of a definite cell *A*-*B*-*C*-*D* termed "working cell" to the electrostatic field induced by the neighboring polarized "driver-cell" *A*′-*B*′-*C*′-*D*′, which acts as electric quadrupole composed of four alternating charges $\rho_{A'}e = \rho_{C'}e = \rho e$ and $\rho_{B'}e = \rho_{D'}e = (1-\rho)e$ arranged on the corners of a square as shown in Fig. 2 (geometrically and electronically the driver-cell is assumed to be identical to the working one) and $\rho_{i'}$ are the population (electronic density) of the site i'. The driver-cell is assumed to admit controllable polarization in such a way that the electronic density ρ can be varied from 0 (empty site) to 1 (center with fully localized excess electron). This can be described by the expression

$$P_{dc} = \frac{\rho'_A + \rho'_C - \rho'_B - \rho'_D}{\rho'_A + \rho'_C + \rho'_B + \rho'_D} = 2\rho - 1, \qquad (2)$$

which defines driver cell polarization and represents normalized excess of the electronic density on one diagonal as compared with that on another diagonal of the cell. Expressing the electronic density in the driver-cell as $\rho = (1+P_{dc})/2$ one obtains the charges of the sites of the driver cells as follows: $q_{A'} = q_{C'} = (1+P_{dc})e/2$, $q_{B'} = q_{D'} = (1-P_{dc})e/2$. These charges interact with the excess electrons of the working cell through the Coulomb forces. The intercell Coulomb energy depends on the distribution of the two electrons in the working cell, we denote such energy as u_{ik} for the distribution (*i*, *k*) in which the two electrons occupy the sites *i* and *k*. Moreover, an essential feature distinguishing bi-dimeric cells from the tetrameric ones is the fact that in case of bi-dimeric cells the intercell Coulomb energies u_{ik} depend not only on the charge configuration (*i*, *k*) in the working cell but also on the mutual arrangement of two interacting cells. Indeed, bi-dimeric cells can be arranged in two different ways. namely, dimers *i*-*k* and *i*′-*k*′ can lie either on the same straight line ("head-to-tail" arrangement of cells) or on the parallel lines ("side-by-side" arrangement of cells) and these two types of arrangements are inequivalent from the point of view of the intercell Coulomb interaction. Figure 2 shows all possible distributions of four charges in the pair of interacting cells for two types of mutual arrangements of cells and four charge configurations (*i*, *k*) of the working cell.

Then by using the schemes shown in Fig. 2 one can find the expressions for the intercell Coulomb energies u_{ik} at different mutual arrangements of the cells. These expressions are listed in Table 1. In these expressions b is the length of side of the square cell, *c* is the distance between the working and driver cells (Fig. 2) and ε is the relative permittivity that is assumed to be the same for intra- and intercell Coulomb interactions. Note that for head-to-tail arrangement of cells these expressions coincide with the earlier reported corresponding expressions found for the case of tetrameric cells [43]. It is also seen

from Table 1, that the energies u_{ik} found for the end-to-end and side-by-side arrangements prove to be equal provided that (i, k) = (A, C) or (B, D) (diagonal-type electronic configurations), while these energies are essentially different if (i, k) = (A, D) or (B, C).

It is quite clear that while constructing various QCA devices (inverters, fanouts, majority logic gates) from such cells, both mutual arrangements of cells are inevitably present within the same device. On the other hand, to ensure proper functionality of the device all pairs of cells must be equivalent in terms of their functional characteristics (e.g. cell-cell response functions). Therefore, an important task is to elucidate the conditions under which the indicated differences in Coulomb energies for different types of mutual arrangement of cells do not lead to a difference in functional characteristics for different pairs of cells. In the subsequent analysis of the properties of bi-dimeric cells we will pay attention to this problem.

Let us define the electronic Hamiltonian of the bi-dimeric working cell subjected to the action of the Coulomb field created by the driver-cell. It is convenient to present the Hamiltonian for a definite type of arrangement (*ta*) of the two cells in the following matrix form

$$\hat{H}_{EL}^{ta}=\begin{array}{c} \begin{matrix} \psi_{AC} & \psi_{AD} & \psi_{BC} & \psi_{BD} \end{matrix} \\ \begin{pmatrix} u_{AC}^{ta} & t & t & 0 \\ t & U+u_{AD}^{ta} & 0 & t \\ t & 0 & U+u_{BC}^{ta} & t \\ 0 & t & t & u_{BD}^{ta} \end{pmatrix} \end{array}, \qquad (3)$$

where *ta* = "head-to-tail" or "side-by-side". This 4×4 – matrix is defined in the basis comprising four states $\psi_{ik}\left(S\right)$, each corresponding to one of the electronic configurations (i, k) and the total spin S, which takes the values 0 and 1 for the two-electron cell. As distinguished from the tetrameric cell for which the Hamiltonian matrices for S=0 and 1 are different [43], these matrices for a bi-dimeric cell are spin independent due to the absence of the magnetic interactions between the electrons of the dimeric half-cells. Therefore the symbol S is omitted in the notation of the basis states and in the notation of the Hamiltonian matrix $\hat{H}_{EL}^{ta}$.

Regarding the Hamiltonian, Eq. (3), the following comment should be done (this comment is inspired by the comment of the Reviewer of *JCP* to the authors). Usually, a MV cell has a net charge (for example, cation-radical systems, Section 5). The working cell feels this total charge even if the driver cell is unpolarized. This charge is usually neutralized by the charge of the counter-ion or the charge from substrate. The emerging problem of the neutralizing charge has been discussed in Ref. [24] devoted to the synthesis of a neutral mixed-valence diferrocenyl carborane for molecular QCA

applications. In this respect one should mention Re. [65] in which an electrostatic model has been suggested that allowed to reveal the character of perturbation induced by the counterion on the metal sites and to the barrier for switching.

The Hamiltonian, Eq. (3), includes only the field of the extra electrons of the driver (and excludes net charge) acting on the working cell that actually arises from the electric quadrupole-quadrupole interactions (interactions of mobile electrons). Since the neutralizing charge can be modeled in different particular ways we will keep a more unified model consideration in which the monopole charges are excluded (the action of the neutralizing charge will be considered elsewhere as applied to the real systems). Nevertheless, the monopole charges are dominating when we consider the difference between side-by-side and head-to-tail geometries subjected to the field of the driver. This circumstance becomes decisive when comparing the functional characteristics such as cell-cell response function evaluated for these two configurations. That is why while representing precise quantum-mechanical calculations of the cell-cell response function, only the case side-by-side arrangement of bi-dimeric square cells is considered.

The vibronic coupling is considered in the framework of the Piepho, Krausz, and Schatz (PKS) vibronic model [45]. One can define four symmetry-adapted PKS vibrations of a bi-dimeric square cell with the following vibrational coordinates:

$$q_{A_1} \equiv q_1 = \frac{1}{2}\left(q_A + q_B + q_C + q_D\right), \qquad q_{A_2} \equiv q_2 = \frac{1}{2}\left(q_A + q_C - q_B - q_D\right),$$
$$q_{B_1} \equiv q_3 = \frac{1}{2}\left(q_A + q_D - q_B - q_C\right), \qquad q_{B_2} \equiv q_4 = \frac{1}{2}\left(q_A + q_B - q_C - q_D\right). \tag{4}$$

These coordinates are the linear combinations of the coordinates q_A, q_B, q_C and $q_D$describing the breathing vibrations of the ligand surroundings of the metal sites *A*, *D*, *C* and *D*. All breathing vibrations are characterized by the only frequency ω that is assumed (according to PKS model) to be independent on whether the site is occupied by the excess electron or it is empty. This means that all symmetry adapted cell vibrations are also characterized by the same frequency ω. The linear combinations in Eq. (7) are the same as in the case of a true tetrameric square cell [43] but they are labeled by the irreducible representation of the C_{2v} point group of the bi-dimeric cell.

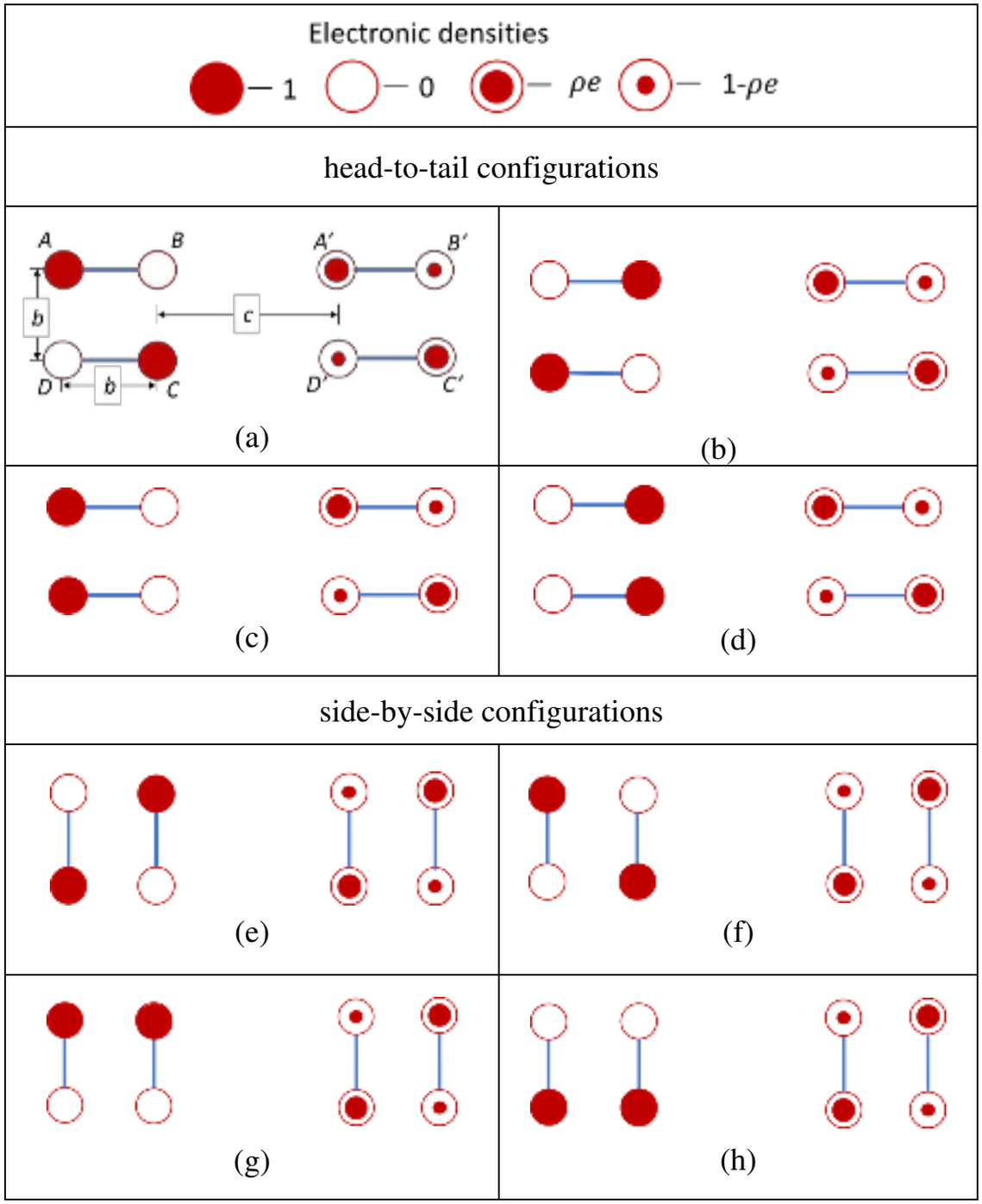

Fig. 2. Four possible distributions of the charges in two interacting cells arranged in the head-to-tail (a, b, c, d) and the side-by-side (e, f, g, h) ways. The charge configurations in the working cell are the following: (A,C) (a, e). (B,D) (b, f), (A,D) (c, g) and (B,C) (d, h). Here A-B-C-D is the working cell, and A'-B'-C'-D' is the driver-cell.

Table 1. Dependences of the intercell Coulomb energies on the electron density ρ in the driver-cell, and the intracell and intercell distances *b* and *c* evaluated for different electronic distributions in the bi-dimeric working cell and two possible mutual arrangements (head-to-tail and side-by-side) of the cells.

Configuration	Energies of intracell Coulomb interactions
$u_{AC}^{head-to-tail}$ $u_{AC}^{side-by-side}$	$\frac{e^2}{\varepsilon}\left[\frac{2\rho}{b+c}+\frac{2(1-\rho)}{\sqrt{(b+c)^2+b^2}}+\frac{1-\rho}{2b+c}+\frac{1-\rho}{c}+\frac{\rho}{\sqrt{(2b+c)^2+b^2}}+\frac{\rho}{\sqrt{b^2+c^2}}\right]$
$u_{BD}^{head-to-tail}$ $u_{BD}^{side-by-side}$	$\frac{e^2}{\varepsilon}\left[\frac{2(1-\rho)}{b+c}+\frac{2\rho}{\sqrt{(b+c)^2+b^2}}+\frac{\rho}{2b+c}+\frac{\rho}{c}+\frac{1-\rho}{\sqrt{(2b+c)^2+b^2}}+\frac{1-\rho}{\sqrt{b^2+c^2}}\right]$
$u_{AD}^{head-to-tail}$	$\frac{e^2}{\varepsilon}\left[\frac{1}{b+c}+\frac{1}{2b+c}+\frac{1}{\sqrt{(b+c)^2+b^2}}+\frac{1}{\sqrt{(2b+c)^2+b^2}}\right]$
$u_{AD}^{side-by-side}$	$\frac{e^2}{\varepsilon}\left[\frac{1}{b+c}+\frac{\rho}{2b+c}+\frac{1-\rho}{c}+\frac{1}{\sqrt{(b+c)^2+b^2}}+\frac{1-\rho}{\sqrt{(2b+c)^2+b^2}}+\frac{\rho}{\sqrt{b^2+c^2}}\right]$
$u_{BC}^{head-to-tail}$	$\frac{e^2}{\varepsilon}\left[\frac{1}{b+c}+\frac{1}{c}+\frac{1}{\sqrt{(b+c)^2+b^2}}+\frac{1}{\sqrt{c^2+b^2}}\right]$
$u_{BC}^{side-by-side}$	$\frac{e^2}{\varepsilon}\left[\frac{1}{b+c}+\frac{1-\rho}{2b+c}+\frac{\rho}{c}+\frac{1}{\sqrt{(b+c)^2+b^2}}+\frac{\rho}{\sqrt{(2b+c)^2+b^2}}+\frac{1-\rho}{\sqrt{b^2+c^2}}\right]$

Figure 3a shows the high-symmetric (reference) molecular structure, that corresponds to the fully delocalized electronic pair when each metal site can be formally regarded as comprising half of electron charge. The assignments of the molecular vibrations to the irreducible representations of the C_{2v} point group correspond to molecular coordinate frame shown in Fig. 3a. The images of symmetry adopted PKS vibrations of a bi-dimeric cell are shown in Figs. 3b-3d. The full-symmetric vibration with the coordinate q_1 represents simultaneous compression or expansion of the coordination spheres of the four metal sites, while the vibrations described by the coordinates q_2, q_3 and q_4 represent compression of some two coordination spheres accompanied by expansion of other two ones. Thus, the coordinate q_2 describes the diagonal-type vibration (Fig. 3c) when two coordination spheres belonging to one diagonal are expanded while the spheres lying on another diagonal are contracted, while the coordinates q_3 and q_4 relate to the side-type vibrations for which the coordination spheres belonging to one side of the square cell are expended while the spheres belonging to opposite side are contracted. (Figs. 3d, 3e).

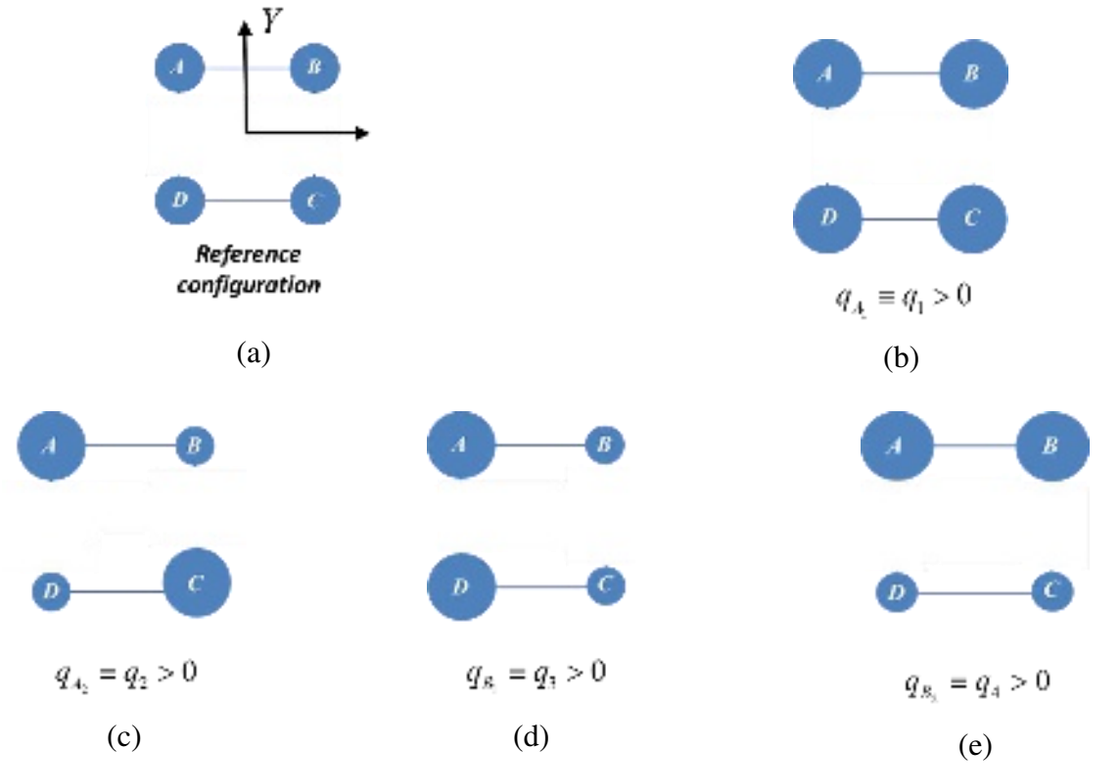

Fig. 3. Images of the symmetry adapted vibrational PKS coordinates of a bi-dimeric cell belonging to the C_{2v} point group: coordinate frame and reference configuration (a); full-symmetric coordinate $q_1 > 0$ (b); coordinate of A_2 symmetry, $q_2 > 0$ (c); coordinate of B_1 symmetry, $q_3 > 0$ (d); coordinate of B_2 symmetry, $q_4 > 0$ (e). Large and small blue balls schematically show the expanded and compressed ligand surroundings of the metal sites, while medium balls indicate reference vibrational configuration. Only positive displacements are shown.

In the study of tetrameric two-electron square cell with violated strong U limit, one faces a complex vibronic problem [43] dealing with three active vibrations described by the coordinates q_2, q_3 and q_4. The-full-symmetric mode with coordinate q_1 proves to be independent of the distributions of the electronic pair and so it can be ruled out from the consideration by the proper choice of the reference structure. In the case of a bi-dimeric square cell the simplest way to derive the vibrationally-dependent part of the Hamiltonian of the bi-dimeric working cell is to extract the corresponding 4×4 block of the 6×6-matrix deduced for the tetrameric cell (Eq. (8) in [43]). This block is that defined in the basis of four electronic configurations allowed in the case of bi-dimeric cell. Keeping the notations adopted in [43] we arrive at the following vibrationally-dependent Hamiltonian matrix for the bi-dimeric cell:

$$\hat{H}_q = \frac{\hbar\omega}{2}\left(q_2^2 + q_3^2 - \frac{\partial^2}{\partial q_2^2} - \frac{\partial^2}{\partial q_3^2}\right)\hat{I}_4 + \upsilon \begin{array}{c} \begin{matrix} \psi_{AC} & \psi_{AD} & \psi_{BC} & \psi_{BD} \end{matrix} \\ \begin{pmatrix} q_2 & 0 & 0 & 0 \\ 0 & q_3 & 0 & 0 \\ 0 & 0 & -q_3 & 0 \\ 0 & 0 & 0 & -q_2 \end{pmatrix} \end{array}, \qquad (5)$$

The first term in Eq. (5) is the Hamiltonian of the free harmonic oscillations and the second term describes the vibronic coupling, where $\hat{I}_4$ is the 4×4 - unit matrix and υ is the vibronic coupling parameter.

It is seen that unlike the case of tetrameric cell for which three-mode vibronic problem arises, only two vibrations are active in the case of bi-dimeric cell, namely, the vibration with the coordinate q_2 occurring with participation of the diagonals *A*-*C* and *B*-*D* (Fig. 3c) and the vibration with the coordinate q_3 involving the sides *A*-*D* and *B*-*C* of the cell (Fig. 3d), while the vibrations with the coordinate q_4 is irrelevant because it is associated with the excluded electronic configurations in which the dimeric subunits are occupied by two electrons. We thus arrive at the two-mode vibronic problem that is described by the full Hamiltonian:

$$\hat{H}_{ta} = \hat{H}_{EL}^{ta} + \hat{H}_q . \tag{6}$$

The forthcoming analysis of the properties of bi-dimeric cells is based on the solution of this two-mode problem performed both in the framework of semiclassical adiabatic approach and with the aid of more exact quantum-mechanical vibronic approach. Particularly, by calculating the wave-function of the ground vibronic state (ground eigenvalue of the Hamiltonian, Eq. (6)) we will evaluate and analyze the low-temperature polarization of the working cell, that is defined by the expression

$$P_{wc} = \frac{\rho_A + \rho_C - \rho_B - \rho_D}{\rho_A + \rho_C + \rho_B + \rho_D}, \tag{7}$$

which looks quite similarly to the expression, Eq. (2), defining the polarization of the driver-cell, but unlike that expression, Eq. (7) includes site-populations ρ_i related to the working cell (unprimed values). The populations ρ_i does depend on the polarization of the driver-cell, thus giving rise to the dependence $P_{wc}\left(P_{dc}\right)$ known as "cell-cell response function" that is a key characteristic of QCA [11].

3. Results and discussion within semiclassical adiabatic approach

In all subsequent sample calculations, we use the following values for the transfer parameter, the intracell and intercell distances and the relative permittivity: t =200 cm^{-1}, b=8Å, c=24Å, ε = 10. We will also use the value $\hbar\omega = 300$ cm^{-1} for the vibrational quantum, while the vibronic coupling parameter υ will be varied in a series of sample calculations.

Let us consider first the case of vanishing vibronic coupling ($\upsilon = 0$), which corresponds to the pure electronic model with the Hamiltonian, Eq. (3). By diagonalizing the energy matrix in Eq. (3) with the above introduced t, b, c and ε values, we obtain the low-temperature (at T=0 K) pure electronic cell-cell response functions shown in Fig. 4. One can see that for both head-to-tail and side-by-side arrangements the cell-cell response proves to be rather weak, which means that even at fully polarized driver-cell the working cell remains almost unpolarized and the cell-cell response function is practically linear. It is

also seen that the cell-cell response proves to be slightly strengthen for side-by-side arrangement of cells. Such weak linear response is evidently due to the fact at chosen set of parameters the Coulomb repulsion is not strong and therefore the shape of the cell-cell response function is far from having required strongly non-linear shape. Indeed, one obtains $U \approx 425$ cm^{-1} with the chosen values of b and ε, and so the inequality $t << U$ is not fulfilled provided that t =200 cm^{-1}.

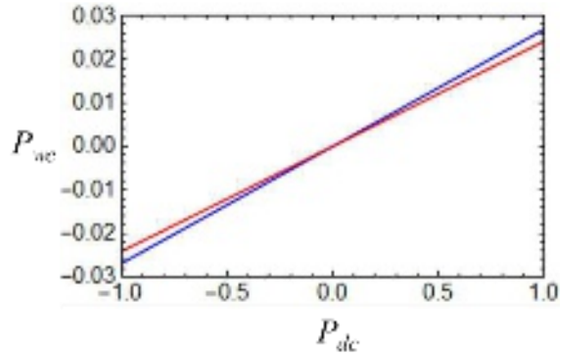

Fig. 4. Purely electronic cell-cell response functions evaluated for side-by-side (blue line) and head-to-tail (red line) arrangements of working and driver cells.

Now let us analyze the effect of the vibronic coupling on the properties of the cell. First, we will analyze the properties of the working cell subjected by the action of unpolarized $(P_{dc} = 0)$ driver-cell. The latter can be regarded as composed of four equal charges $e/2$ located at the metal centers. As distinguished from the strong U limit when the electrostatic field created by unpolarized driver-cell does not influence the electronic distributions in the working cell, in more general case when the strong U limit is violated such field does produce considerable effect on the electronic density distribution because of inequivalence of different side-type distributions with respect to the applied field.

First, we will focus on the lower adiabatic potential surface of the working cell on the strength of the vibronic coupling. The adiabatic potentials represent the eigenvalues of the Hamiltonian, Eq. (6), evaluated in the framework of adiabatic semiclassical approximation which assumes that the kinetic energy of vibrations is neglected. The shapes of the lower adiabatic potential surface evaluated at different values of the vibronic coupling parameter for the two arrangements of cells are shown in Figs. 5 and 6. For a relatively strong vibronic coupling (Figs. 5a and 6a) the adiabatic potential surface has four minima. Two of them are the global equivalent minima, which correspond to the predominant localization of the electronic pair on a certain diagonal of the cell, while the other two are excited minima in which the adiabatic wave functions describe the predominant localization of electrons on the sides *A*-*D* and *B*-*C*. Note that for side-by-side arrangement the excited minima are energetically equivalent (Fig. 5a), while for head-to-tail arrangement the excited minimum corresponding to the localization of electrons on the distant side *A*-*D* is deeper than the excited minimum in which the electrons are

predominantly localized on the closely spaced *B*-*C* side. As a result, in the case of a head-to-tail arrangement of cells, the contribution of the (*A*, *D*) electronic distribution to the adiabatic wave function at the global minimum turns out to be significant, which leads to a decrease in the contribution of the diagonal electronic distributions. As the vibronic coupling decreases, the two global minima approach each other and the barrier between them diminishes. Simultaneously, in the case of side-by-side arrangement the two equivalent excited minima become shallower and at some strength of the vibronic coupling they disappear and the adiabatic potential surface having four minima is transformed into the double-well surface (Fig. 5b).

In the case of head-to-tail arrangement, the disappearance of the excited minima upon decreasing of the strength of the vibronic coupling occurs in two steps. First, the decrease of υ leads to disappearance of the highest excited minimum corresponding to the localization of the electronic pair on the closely spaced *B*-*C* side (Fig. 6b). Then, at lower value of υ the deeper excited minimum in which electronic pair is localized on the distant side *A*-*D* disappears as well and the adiabatic potential surface acquires a double-well shape (Fig. 6c). Finally, at further decrease of the vibronic coupling the two minima are getting more and more shallow and approach each other and at some critical value of υ (that depends on the type of arrangement) the two minima merge and the adiabatic potential surface is transformed into the single-well one (Figs. 5c and 6d). The adiabatic wave-function in this only minimum coincides with the wave-function obtained in the framework of pure electronic approach and describes the electronic pair predominantly delocalized over two diagonal positions, but this wave-function also contains a significant contribution of side-type configurations due to the fact that the considered situation is far from the strong *U* limit.

Additional insight into the evolution of the global minima with changing of the vibronic coupling parameter is provided by Fig. 7, which shows the comparison of the coordinates of the minima evaluated as functions of the vibronic coupling parameter for the working cell subjected by the Coulomb field of unpolarized driver-cell for two kinds of possible arrangements of the cells. It is seen from Fig. 7a that

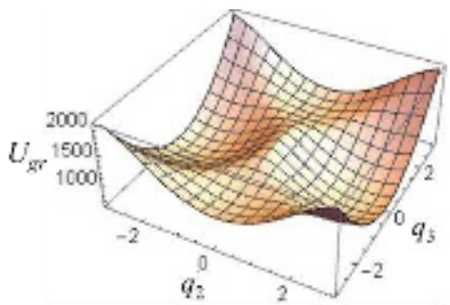

(a)

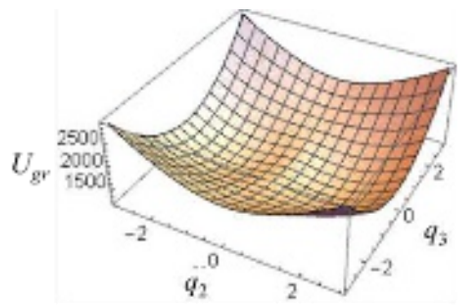

(b)

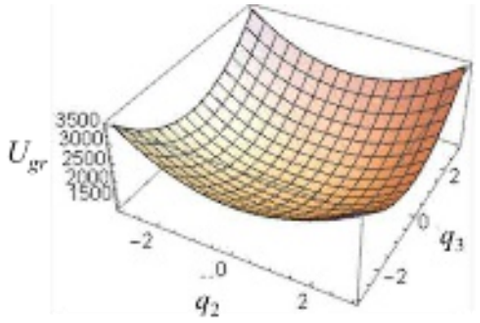

(c)

Fig. 5. Lower sheet of the adiabatic surface of bi-dimeric working cell subjected to the Coulomb field of unpolarized driver-cell ($P_{dc} = 0$) evaluated for side-by-side arrangement of interacting cells. with the following values of the vibronic coupling parameter: $\upsilon = 700\,\mathrm{cm}^{-1}$(a), $\upsilon = 400\,\mathrm{cm}^{-1}$(b), $\upsilon = 200\,\mathrm{cm}^{-1}$(c).

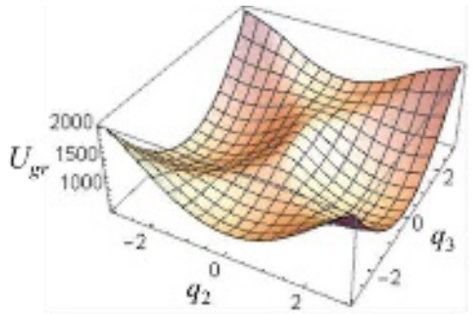

(a)

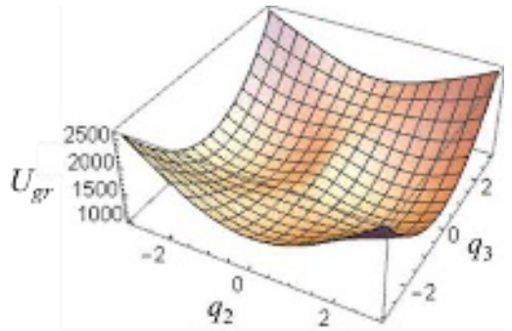

(b)

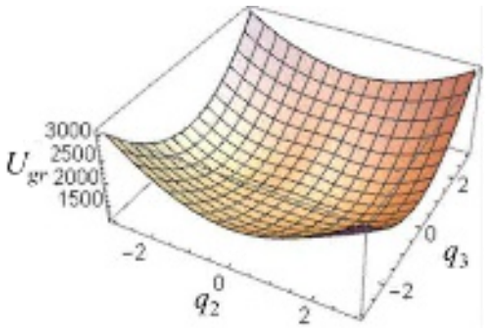

(c)

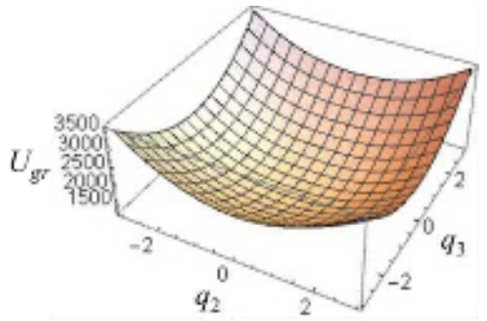

(d)

Fig. 6. Lower sheet of the adiabatic surface of bi-dimeric working cell subjected to the Coulomb field of unpolarized driver-cell ($P_{dc} = 0$) evaluated for head-to-tail arrangement of interacting cells with the following values of the vibronic coupling parameter: $\upsilon = 700\,\mathrm{cm}^{-1}$(a), $\upsilon = 500\,\mathrm{cm}^{-1}$(b), $\upsilon = 350\,\mathrm{cm}^{-1}$(c), $\upsilon = 200\,\mathrm{cm}^{-1}$(d).

for side-by-side arrangement of cells the transformation of the adiabatic potential surface having the only minimum to the surface having two equivalent ground minima occurs at lower value of υ than in the case of head-to-tail arrangement. This is evidently due to the fact that head-to-tail arrangement

promotes stronger contribution of the side-type electronic configuration (namely, of that in which electronic pair occupies the remote side *A*-*D* in the working cell). Also, as a result of the asymmetry of the two side-type configurations induced by the intercell Coulomb interaction in the case of head-to-tail arrangement the coordinate q_3^{min} in this case undergoes slight shift from zero at moderate vibronic coupling (Fig. 7b), while for side-by-side arrangement $q_3^{min} = 0$ independently of the strength of the vibronic coupling because in the latter case both side-type configurations are energetically equivalent. Note that aforenamed difference between the coordinates of the minima disappears in the limit of strong vibronic coupling. This can be explained by the fact that in this limit only diagonal-type electronic distributions contribute sizably to the wave-functions in the global minima, which are fully indifferent to the type of cells arrangement.

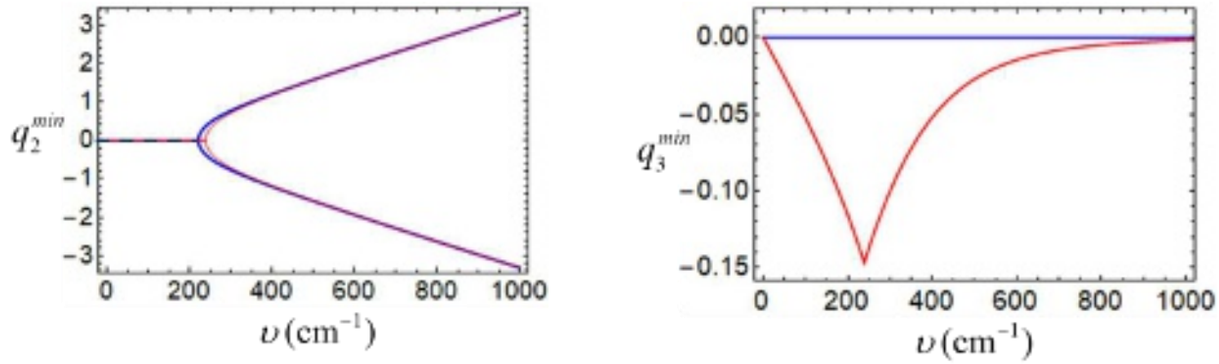

(a) (b)

Fig. 7. Dependences of the coordinates q_2^{min} (a) and q_3^{min} (b) of the ground minima of the lower adiabatic potential surface of the working cell subjected by the Coulomb field of unpolarized driver-cell ($P_{dc} = 0$) on the value of the vibronic coupling parameter evaluated for side-by-side (blue lines) and head-to-tail (red lines) arrangements of the interacting cells.

Figure 8 shows the populations of different pairs of metal centers by the two excess electrons calculated in the global minima of the lower adiabatic potential surface of the working cell subjected to the Coulomb field of unpolarized driver-cell as functions of the vibronic coupling for two kinds of cells arrangement.

For weak vibronic interaction (left part of Fig. 8) when the adiabatic potential has the only minimum the electronic pair populations in this minimum are practically independent of υ and close to the populations calculated with the aid of pure electronic model. In this case the electronic pair is mainly delocalized over two diagonals of the cell ($\rho_{AC} = \rho_{BD} \approx 0.37$ for side-by-side arrangement and $\rho_{AC} = \rho_{BD} \approx 0.35$ for head-to-tail arrangement) and with less extent occupy the side positions ($\rho_{AD} = \rho_{BC} \approx 0.13$ for side-by-side arrangement and $\rho_{AD} \approx 0.23$, $\rho_{BC} \approx 0.07$ for head-to-tail arrangement). As distinguished from side-by-side arrangement for which both side-type populations are equal, in the case

of head-to-tail arrangement the side *A*-*D* is populated to much higher extent than the side *B*-*C* due to the inequivalence of these two sides with respect to intercell interaction. It is seen that the total side-type population $\rho_d = \rho_{AD} + \rho_{BC}$ proves to be higher for side-by-side arrangement and consequently the overall diagonal-type population $\rho_s = \rho_{AC} + \rho_{BD}$ is diminished in this case as compared with that occurring for head-to-tail arrangement. This is just the reason why for side-by-side arrangement of cells the transformation of the single-well surface to the double-well one occurs at lower value of υ than for head-to-tail arrangement.

For υ lying above the critical value corresponding to the transition from the single-well surface to the double-well surface, the electronic densities in the two ground minima depend on υ in such a way that the increase of υ tends to localize the electronic pair on a certain diagonal of the cell (for the minimum considered in Fig. 8 this is the diagonal *A*-*C*), while the populations of other diagonal and of the two sides of the cell go to zero (right side of Fig. 8). Although the slopes of the $\rho_{ij}(\upsilon)$ curves are bigger for side-by-side arrangement than for head-to-tail one this difference is getting less pronounced with the increase of υ. Finally, in the limit of strong vibronic coupling, the electronic pair tends to be fully localized on the diagonal *A*-*C* ($\rho_{AC} \approx 1$) for both types of arrangements. Note that at strong vibronic coupling the difference between the electronic density distributions for two of arrangements becomes insignificant. Physically this means that for such strong vibronic coupling the role plays only the diagonal-type distributions which are insensitive to the type of arrangement. In other words, at strong vibronic coupling, we arrive at the situation that is typical for strong *U* limit, for which only the diagonal configurations are involved into the game and hence the type of arrangement does not play any role. One can thus conclude that even if the Coulomb repulsion does not reach the strong *U* limit, a strong enough vibronic coupling can produce the same effect of localization as the intracell Coulomb repulsion and consequently can create an appreciable barrier, which separates two distinct charge configurations encoding binary information thus ensuring bi-stability of the cell.

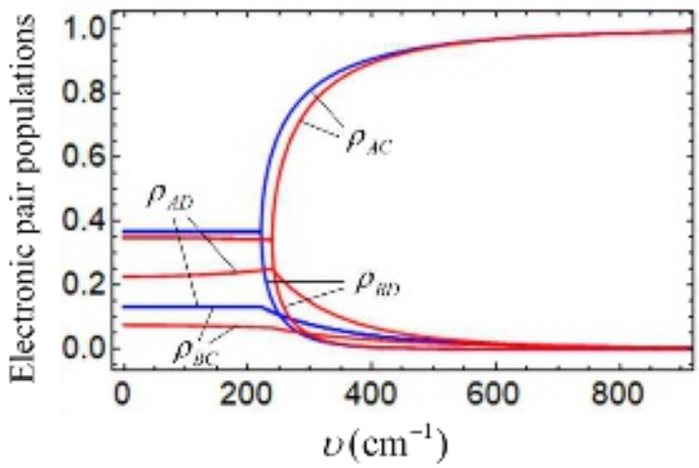

Fig. 8. Electronic pair occupancies in the global minimum of the lower adiabatic potential surface evaluated for working cell subjected to the action of unpolarized driver-cell as functions of the vibronic coupling parameter. The dependences calculated for side-by-side and head-to-tail arrangements of the interacting cells are shown by blue and red lines, respectively. For the range of υ for which the potential surface is of double-well shape, only the pair populations in one minimum are presented, while the populations in another minimum can be found by interchanging $\rho_{AC} \rightleftarrows \rho_{BD}$.

It is also notable that in each deep global minimum in the case of strong vibronic interaction the working cell proves to be fully polarized even provided that the driver-cell is unpolarized. This is "broken symmetry polarization" rather than the genuine polarization of the cell because in two global minima the cell acquires different polarizations ($P_{wc} = -1$ and $+1$) and so the average polarization is zero. Nevertheless, such broken symmetry polarization can be easily transformed into the genuine polarization of the working cell under the action of the polarized driver-cell. Indeed, the quadrupole electrostatic field of the driver cell breaks down the equivalence of the two global minima stabilizing a selected minimum and destabilizing another one, and so the working cell acquires a definite polarization that is already "prepared" by the vibronic interaction. This is illustrated in Fig. 9 presenting the effect of the electrostatic field of the driver-cell on the populations of different pairs of metal centers by the two excess electrons evaluated in the global minimum of the lower potential surface of the working cell at different values of the vibronic coupling-parameter. Indeed, at relatively strong vibronic coupling the population ρ_{AC} discontinuously changes from $\rho_{AC} \approx 0$ to $\rho_{AC} \approx 1$ (curves 5 in Figs. 9a, 9b), while the polarization ρ_{BD} changes from $\rho_{BD} \approx 1$ to $\rho_{BD} \approx 0$ (curves 5 in Figs. 9c, 9d) upon changing polarization P_{dc} from negative to positive values. This is because at $P_{dc} < 0$ the global minimum is that in which

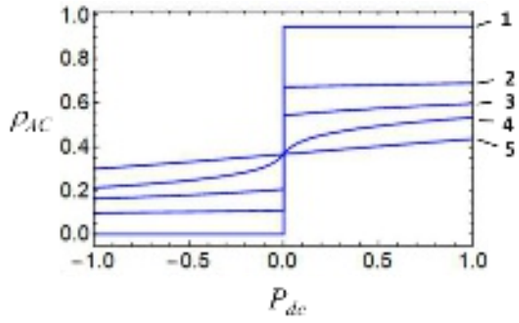

(a)

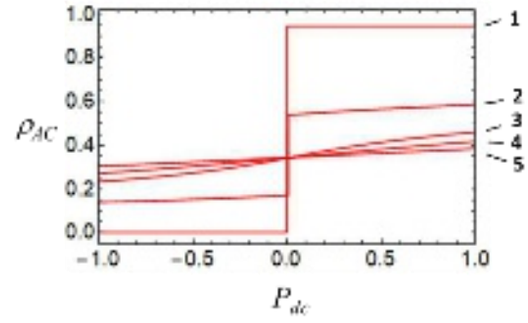

(b)

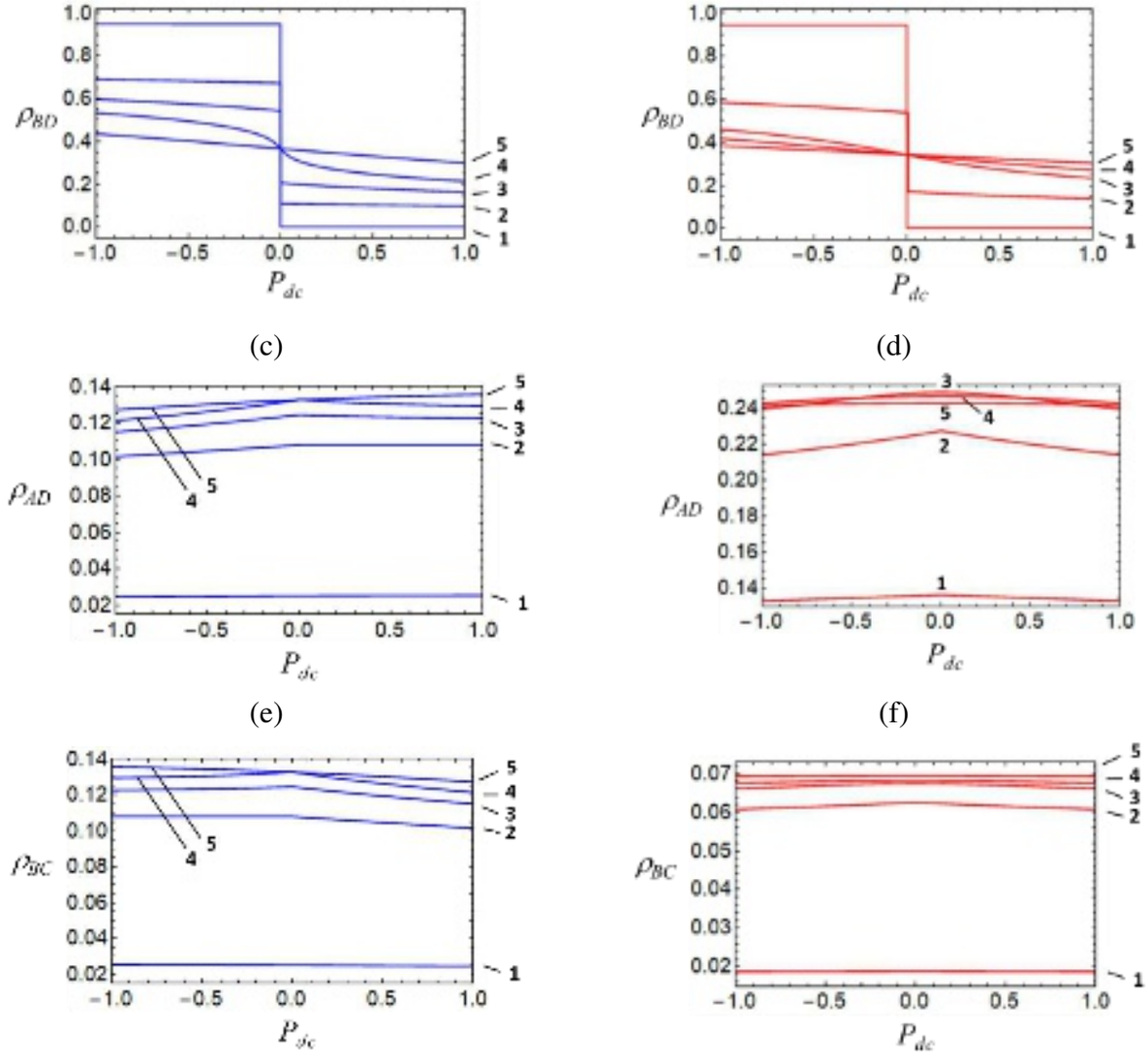

Fig. 9. Electronic pair occupancies in the global minimum of the lower adiabatic potential surface of the working cell evaluated as functions of the polarization of driver-cell for the following five values of the vibronic coupling parameter: curves 1 – $\upsilon = 500$ cm^{-1}, 2– $\upsilon = 250$ cm^{-1}, 3 – $\upsilon = 230$ cm^{-1}, 4 – $\upsilon = 220$ cm^{-1}, 5 – $\upsilon = 200$ cm^{-1}. The dependences calculated for side-by-side ((a), (c), (e), (g)) and head-to-tail ((b), (d), (f), (h)) arrangements of the interacting cells are shown by blue (left side) and red (right side) lines, respectively.

electronic pair is almost fully localized on the diagonal *B*-*D*, while at $P_{dc} > 0$ another minimum is stabilized in which the pair is localized on the diagonal *A*-*C*. At the same time for such strong vibronic coupling the populations of the side positions remain close to zero and almost insensitive to the field of the driver cell (curves 5 in Figs. 9e, 9g,9h). The only exclusion is the population of the *A*-*D* side in the case of head-to-tail arrangement, which remains still significant at $\upsilon = 500$ cm^{-1} (curve 5 in Fig. 9f) due to strong separation of this side from the driver-cell. At stronger vibronic interaction the latter population becomes vanishing as well (the case is not shown in Fig. 9). Inspection of the dependences calculated

with at $\upsilon = 500$ cm^{-1} allows us to conclude that at strong vibronic coupling the difference between the two types of arrangements tends to disappear. This means that at strong vibronic coupling the cell behaves in the same way as under the condition of strong U limit, i. e. it demonstrates bi-stability and high polarizability.

The weaker is the vibronic interaction the lower is the discontinuous change of the populations of the diagonal positions occurring when polarization P_{dc} passes through zero changing from negative to positive values (compare the curves 1 and 2 in Figs. 9a-9d). This is because at weaker vibronic coupling the minima are shallower and the extent of the population of the diagonal positions in the minima is lower. Also, the contributions of the side populations go up with the decrease in the strength of the vibronic coupling (compare the curves 1 and 2 in Figs. 9e-9h) and the difference between the dependences evaluated for two types of arrangement become more pronounced.

The stepwise character of the dependences disappears at weaker vibronic coupling at which a single-well potential surface arises instead of double-well one provided that the driver-cell is unpolarized. In this single minimum the electronic pair is predominantly delocalized over two diagonal positions, but also the adiabatic wave-function in the minimum contains considerable side-type admixture. In this case upon polarization of the driver cell the single minimum is shifted and undergoes additional stabilization, while the populations of the diagonal positions show gradual dependence on P_{dc} (curves 4 and 5 in Figs. 9a, 9c and curves 3, 4, 5 in Figs. 9b and 9d). In this range of the vibronic coupling the difference between two arrangements is most pronounced because for side-by-side arrangement the double-well surface is transformed to the single-well one at smaller υ - value than for head-to-tail arrangement (Figs. 7 and 8). This explains why, for example, at $\upsilon = 230$ cm^{-1} the diagonal populations show discontinuous change for side-by-side arrangement (curves 3 in Figs. 9a and 9c) and gradual change for head-to-tail one (curves 3 in Figs. 9b and 9d). Finally, at weak enough vibronic coupling all dependences become weak and practically linear (see, for example curves 5) indicating thus that in this case the field of the driver-cell enables to efficiently polarize the working cell. This is evidently due to the fact that at such weak vibronic interaction the violation of the strong U limit becomes critical thus hindering the efficient functioning of such cells in QCA devices. It is to be underlined that the model employed in this section does not take into account the monopole charges of the driver and neutralizing charge as has been already mentioned. Application of the model to the real objects requires adaptation of the model to take into account action of these charges.

4. Quantum -mechanical results

In principle, using the calculated dependences of the electronic pair occupancies in the global minimum on the polarization of the driver-cell shown in Fig. 9 one can evaluate the low-temperature semiclassical cell-cell response functions $P_{wc}\left(P_{dc}\right)$. Nevertheless, providing qualitatively satisfactory

description of the polarization properties of QCA cells, such semiclassical consideration does not allow to perform correct quantitative evaluation of such properties for arbitrary ranges of parameters due to the fact that adiabatic approximation works well only provided that the barrier separating the adiabatic potential minima is very high and so the quantum tunneling of the excess electrons through this barrier is suppressed [37]. In contrast, in the case of moderate vibronic coupling when the barrier between the two minima is less pronounced, the quantum tunneling becomes rather significant. In the latter case the adiabatic approximation fails to correctly describe the polarization properties. Such shortcomings of the semiclassical description turn out to be especially significant when the minima are so shallow that the ground vibronic level lies above the barrier. It is important to note that the shape of the cell-cell response function in its central non-linear part (just responsible for switching of the cell) is of the primary importance for the proper action of a QCA gate and therefore the degree of accuracy of the evaluation in this area is decisive in assessing the applicability of the approach for the theoretical modeling. Nevertheless, the adiabatic approximation fails just in the description of this critical area (see discussion in Ref. [37]).

That is why we will analyze the $P_{wc}\left(P_{dc}\right)$ dependences evaluated in the framework of more precise quantum-mechanical (dynamic) vibronic approach, which takes into account the kinetic energy of molecular vibrations. To solve the dynamic vibronic problem, we present the full Hamiltonian, Eq. (6), in the matrix form using the basis composed of the products $\psi_{ik}|n_2 n_3\rangle$, where $|n_2 n_3\rangle$are the wave functions of the two-dimensional harmonic oscillator, and n_2, n_3 are the vibrational quantum numbers related to the two active types of vibrational modes.

By diagonalizing such matrix, we obtain a set of vibronic energies ε_k of the working cell and the corresponding vibronic wave-functions $\left|k\right\rangle$. The latter are obtained as superpositions

$$|k\rangle = \sum_{i,j,n_2,n_3} c^k(i,j,n_2,n_3)\psi_{ij}|n_2 n_3\rangle, \qquad (8)$$

where the coefficients $c^k(i,j,n_2,n_3)$ depend on parameters U, t, $\upsilon, \hbar\omega$, and also on the driver-cell polarization P_{dc}. Also, these coefficients do depend on the type of mutual arrangement of working and driver cells. To find a numerical solution of the dynamic problem the infinite vibronic matrix has to be truncated. Since both vibrations in PKS model have the same frequencies ω (that is the frequency of the "breathing" vibration of the redox site) we are dealing with the bi-dimensional oscillator coupled to four electronic states so that the total degeneracy of Hilbert space is $G(N) = 2(N+1)(N+2)$, where N is the number of the vibrational levels $n = n_2 + n_3$ involved in the basis set. The truncation for N=10 ensures a good convergence and satisfactory accuracy in the evaluation of the low-lying

vibronic levels involved in the charge reorganization. The accuracy has been additionally controlled for each sets of parameters.

We will focus on the ground vibronic state $|k=1\rangle$ that is the only state that plays role in the evaluation of the cell-cell response function in the low-temperature limit, i. e. at T=0 K. First, we will evaluate the total probabilities of the diagonal-type and side-type two-electron populations in the working cell provided that the driver-cell is unpolarized (P_{dc} .= 0). These probabilities are defined as follows:

$$\rho_d = \rho_{AC} + \rho_{BD} = \sum_{(i,j) = (A,\,C),(B,\,D)} \sum_{n_2,n_3} \left(c^1(i,j,n_2,n_3)\right)^2,$$

$$\rho_s = \rho_{AD} + \rho_{BC} = \sum_{(i,j) = (A,\,D),(B,\,C)} \sum_{n_2,n_3} \left(c^1(i,j,n_2,n_3)\right)^2. \qquad (9)$$

In this context a significant difference between the semiclassical and quantum-mechanical vibronic states should be emphasized. As distinguished from broken symmetry Born-Oppenheimer states, describing predominant localization of the excess electrons on a certain diagonal in the case of the double-well adiabatic potential surface at strong or moderate vibronic coupling, each quantum-mechanical vibronic state contains equal contributions of both diagonal-type states, i. e. in this case one deals with true symmetry. Indeed, at strong vibronic coupling this ground state can be regarded in terms of quantum tunneling between the two equivalent deep minima. For this reason, within the quantum-

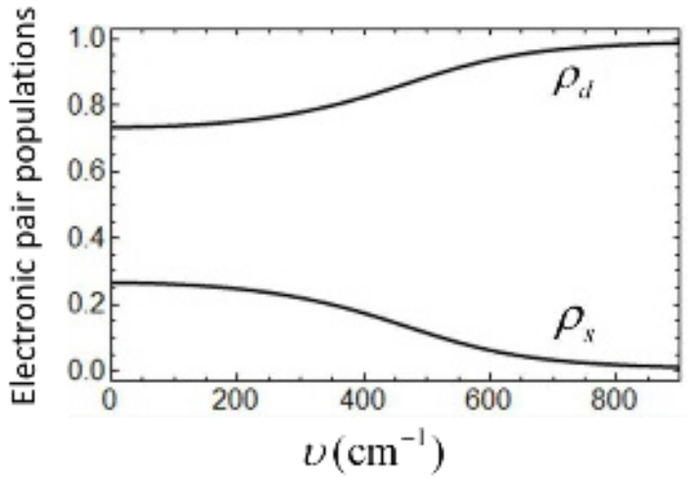

Fig. 10. Total diagonal-type and side-type electronic pair populations in bi-dimeric cell subjected by the electrostatic field of unpolarized driver-cell calculated as functions of the vibronic coupling parameter with the aid of quantum-mechanical vibronic approach. These populations are evaluated for side-by-side arrangement.

mechanical approach it is reasonable to analyze the total probabilities ρ_d and ρ_n rather than the particular probabilities (ρ_{AC} etc.) provided that the working cell is subjected to the field of unpolarized driver-cell, which does not lift the degeneracy of the two global minima.

Figure 10 shows the dependences of ρ_d and ρ_s on the vibronic coupling parameter evaluated for for side-by-side arrangement of cells. For weak vibronic coupling the populations ρ_d and ρ_s are almost independent of υ, and they do not satisfy the inequality $\rho_d >> \rho_s$ because of violation of strong U limit in the case under consideration. At higher vibronic coupling the populations ρ_d and ρ_s become strongly dependent on υ, with ρ_d being the increasing function of υ and ρ_s being the decreasing one. Finally, at sufficiently strong coupling the probabilities reach the values $\rho_d \approx 1$ and $\rho_s \approx 0$ indicating thus that at such strong vibronic coupling the populations coincide with those in the strong U limit. This observation is in line with the above conclusion derived from the semiclassical consideration according to which the strong vibronic interaction acts as a factor effectively restoring the strong U limit in the case when the condition $U >> t$ is not fulfilled. Thus, one can conclude that strong vibronic coupling leads to a "recovery" of electronic density distribution peculiar to the strong U limit.

The above conclusion is confirmed by a series of quantum-mechanical cell-cell response functions (Fig. 11) calculated for side-by-side cells arrangement (as motivated in Section at different values of the vibronic coupling parameters. One can see that at strong vibronic coupling even small driver-cell

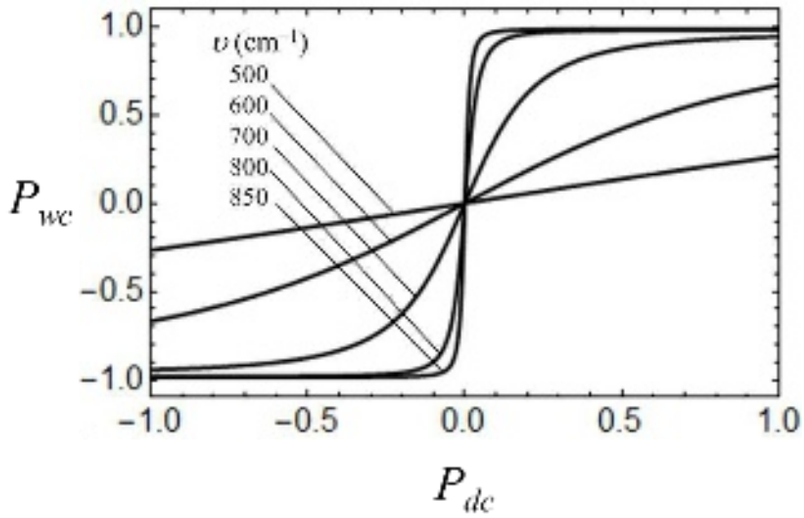

Fig. 11. Series of cell-cell response functions evaluated in the low-temperature limit using quantum-mechanical vibronic approach for side-by-side arrangement of bi-dimeric square cells with different values of the vibronic coupling parameters shown in the plot.

polarization leads to the full polarization of the working cell. Such stepwise strongly nonlinear shape of cell-cell response function is a characteristic feature of QCA that is peculiar for the strong U limit. This evidences that the range of electronic parameters required for suitable functioning of cells should be reconsidered in the sense that at strong vibronic coupling an insufficiently strong Coulomb repulsion is not an insurmountable obstacle for creating QCA cells. The steepness of the cell-cell response function is diminished with decreasing of the vibronic interaction. It is also seen that the maximal attainable value of $|P_{wc}|$ ($|P_{wc}|$ at $|P_{dc}| = 1$) decreases with the decrease of υ. Thus, the working cell admits full polarization at υ =850 cm^{-1} and 800 cm^{-1}, while at smaller values of υ even maximal field of the driver-cell is unable to fully polarize the working cell. Finally, further decrease of the vibronic coupling leads to a weak and almost linear cell-cell response functions. Indeed, the vibronic barrier in this case is too low to produce efficient trapping of the electronic pair and hence the excess electrons are hardly polarizable by the field of the driver-cell.

5. Examples of bi-dimeric square cells with weak and moderate Coulomb repulsion and strong vibronic coupling: analysis based on *ab initio* calculations

While in previous sections we have dealt with general theoretical analysis based on the sets of sample parameters, in this Section we will attempt to answer the question about estimates related to real systems. As building blocks for designing bi-dimeric molecular cell we will employ the polycyclic derivatives of norbornadiene C_7H_8 with two C=C chromophores incorporated in the rigid polycyclic frame whose electronic structure has been studied in detail in Ref. [66] along with the vibronic coupling. In context of the present work this choice is determined by at least three circumstances. First, the norbornylogous bridge compounds can be oxidized so that their cation-radical forms represent MV dimers with the terminal C=C chromophores playing the role of redox sites. Second, the controllable length of the rigid polycyclic bridge allows to compare the functional properties of the bi-dimeric cells with different rationally varying sets of the key electronic parameters. Finally, the high-level *ab initio* results for the series of MV norbornylogous compounds have been mapped onto the frame of the parametric model [66] involving electron transfer and vibronic coupling, i.e. just of the model of a MV dimer employed in the present study.

Fig. 12. Two polycyclic derivatives of norbornadiene (**II** and **III** in notations of Ref. [66]) considered in this Section.

Here we will consider cation-radicals of the two polycyclic derivatives of norbornadiene $[C_{12}H_{12}]^+$ and $[C_{17}H_{16}]^+$ which are shown in Fig. 12. These two MV dimers will be regarded as dimeric half-cells suitable to compose the square cells comprising two extra charges. *Ab initio* CASSCF calculations shows that the symmetric structure of these MV dimers is unstable so that in optimized geometries the positive charges are located mainly at the terminal chromophores. It has been also shown [66] that the out-of-phase "breathing" mode (PKS vibration) is associated with the terminal C=C bonds and predominantly contributes to the potential barriers separating localized structures. *Ab initio* data show that such barriers are quite significant (4609cm^{-1} and 6062 cm^{-1}) thus ensuring strong localization of the extra charge. From the *ab initio* data one can also derive the PKS frequencies, transfer parameters and the vibronic coupling parameters (see details in Ref. [66]), which are collected

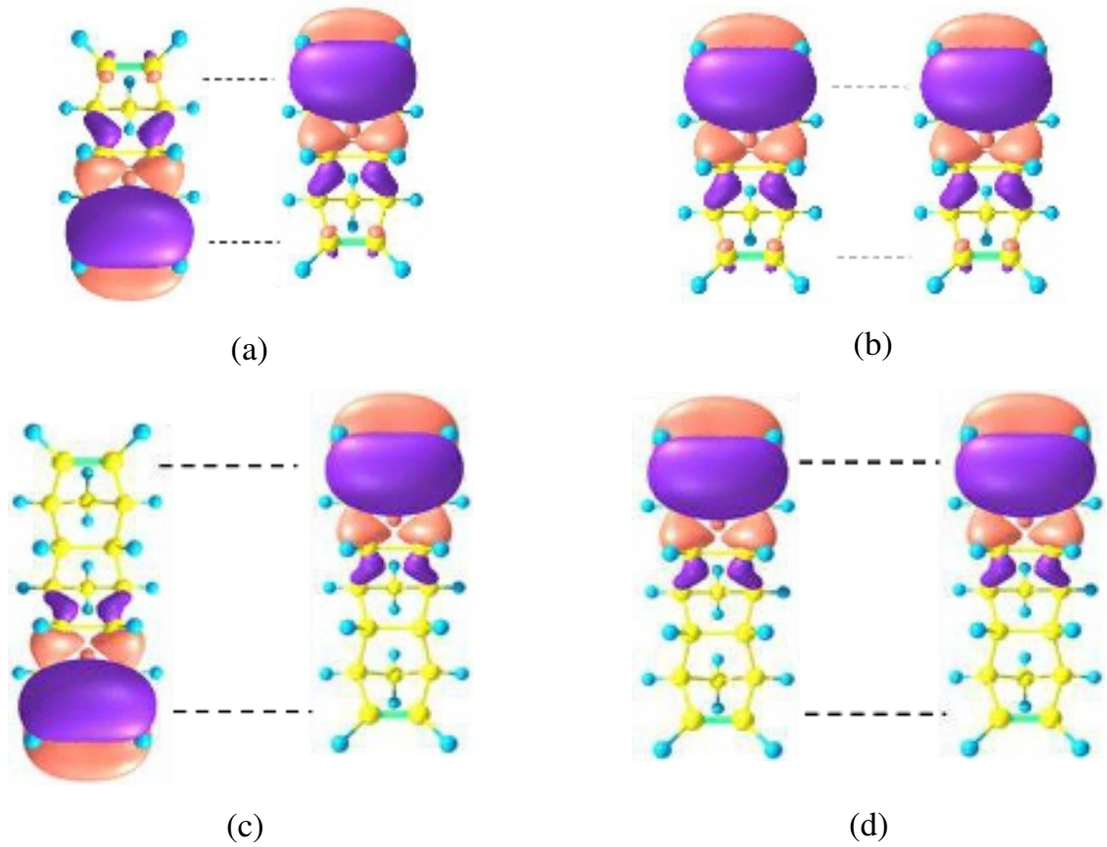

Fig. 13. *Ab initio* based illustration for the two types of charge localized Coulomb configurations (diagonal type and side type) in the bi-dimeric cells composed of the cation-radicals $[C_{12}H_{12}]^+$ ((a) and (b)) and $[C_{17}H_{16}]^+$ ((c) and (d)).

in Table 2. The electronic structures of the two bi-dimeric cells built from cation-radicals $[C_{12}H_{12}]^+$ and $[C_{17}H_{16}]^+$ are illustrated in Fig. 13 with the emphasis on the two Coulomb configurations (diagonal type and side type) of the cells. Since the considered cell has square-planar structure, the distances

between the constituent dimers are equal to the distances *b* between the redox sites (terminal C=C) in the dimers.

Using these data one can estimate the Coulomb parameter U that is in the focus of our consideration (Table 2). Examining the parameters collected in Table 2 one can see that both cells exhibit rather strong (dimensionless coupling $\upsilon/\hbar\omega > 3$) and close in magnitude vibronic interactions, while the ratio U/t proves to be twice higher for cell composed of $[C_{17}H_{16}]^+$ molecules due to the fact that the electron transfer decreases much faster with the increase of the length of the bridge than the intracell Coulomb gap. The obtained ratios U/t shows that for $[C_{12}H_{12}]^+$ based bi-dimeric cell the values *U* and *t* are comparable (*U*/*t*=1.47), while for $[C_{17}H_{16}]^+$ based bi-dimeric cell the ratio *U*/*t*=3.1. These estimations show that the condition of a strong Coulomb repulsion limit ($U >> t$) is evidently violated for both types of cells.

Table 2. Parameters of the bi-dimeric square-planar cells composed of polycyclic derivatives of oxidized norbornadiene playing the role of half-cells. The parameters t , $\hbar\omega$ and υ for two polycyclic derivatives have been calculated with the aid of *ab initio* CASSCF approach [65], the Coulomb gap *U* has been estimated using distance *b* between the redox sites.

Parameters \ Half-cell	$[C_{12}H_{12}]^+$	$[C_{17}H_{16}]^+$
b, Å	4.736	6.973
t, cm^{-1}	4869	1573
$\hbar\omega$, cm^{-1}	1584	1605
υ, cm^{-1}	5282	4924
$\upsilon/\hbar\omega$	3.33	3.07
U, cm^{-1}	7180	4876
U/t	1.47	3.10

To check to what extent strong vibronic coupling is able to ensure high polarizability of the two considered cells we have evaluated the quantum-mechanical cell-cell response functions (see Section

4) with the set of parameters given in Table 2 and also by using the values c=3b for the intercell distances. Due to cationic character of the complexes, we will analyze here only side-by-side arrangement of cells, which is less influenced by the neutralizing charge (Section 2). One can see (Fig. 14) that for both considered types of cells the cell-cell responses are strong and nonlinear. We thus arrive at the conclusion that the vibronic interaction is efficient in the recovering of the cell functionality even under the condition of moderate or even weak Coulomb repulsion.

At the same time the saturation values of cell-cell response function calculated for cells composed of $[C_{17}H_{16}]^+$ dimers prove to be higher than that obtained for cells built from the $[C_{12}H_{12}]^+$ half-cells. Indeed, polarization of the working cells consisting of the $[C_{17}H_{16}]^+$ molecules shows discontinuous change at a weak polarization of the driver-cell upon which the working cell becomes fully polarized. These cells looks as ideal from the point of view of their functionality in QCA devices, while for cells built from the $[C_{12}H_{12}]^+$ molecules the steepness of the abrupt change of polarization of the working cell proves to be slightly lower and also saturation value of $|P_{wc}|$ does not reach 1.

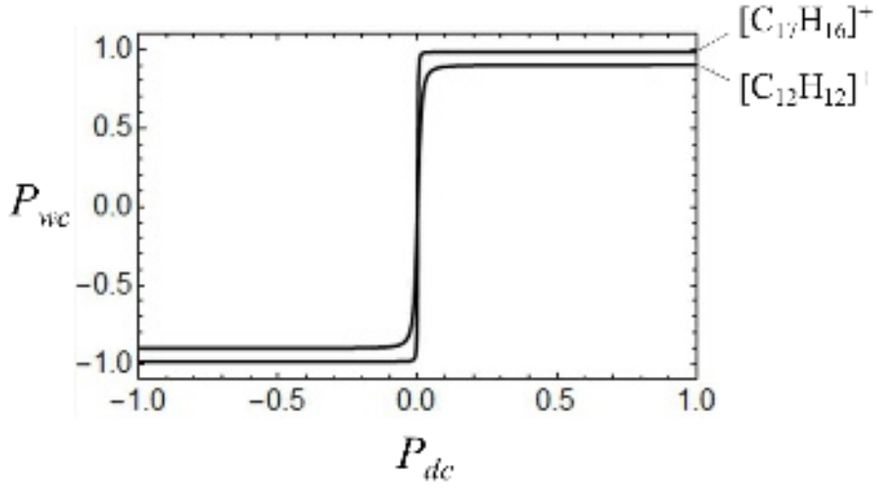

Fig. 14. Cell-cell response functions calculated for side-by-side arrangement of bidimeric square cells composed of either two $[C_{12}H_{12}]^+$ or two $[C_{17}H_{16}]^+$ MV molecules with the set of parameters listed in Table 2 and c=3b.

In order to prove that even for cells composed of $[C_{17}H_{16}]^+$ compounds the parametric regime is far from the strong U limit we have presented in Fig. 15 the cell-cell response function calculated for such cells together with the cell-cell response function evaluated for hypothetical cells having the same set of parameters with the exception of the vibronic coupling parameter that is reduced from its real value 4924 cm^{-1} (solid line) to the value $\upsilon = 3000\ cm^{-1}$. This moderate variation of the vibronic coupling leads to a dramatic change in the shape of the cell-cell response function. It is seen that as distinguished from the cell-cell response function found for cells consisting of $[C_{17}H_{16}]^+$ dimers the functions for hypothetical cells describe weak and nearly linear response, which is

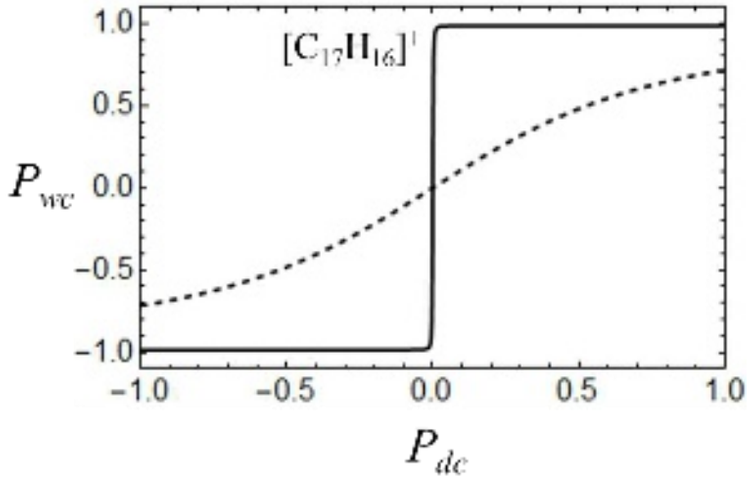

Fig. 15. Comparison of cell-cell response function calculated for the bidimeric square cells composed of two $[C_{17}H_{16}]^+$ MV molecules (solid line) with that calculated for hypothetical bi-dimeric square cells possessing the same values of the parameters except the vibronic coupling parameter that is reduced from 4924 cm^{-1} (solid line) to $\upsilon = 3000\ cm^{-1}$ (dashed line). Both functions are evaluated assuming side-by side arrangements of cells.

indicative of considerable contributions of side-type charge configurations. One can thus conclude that the strong *U* limit is not reached for the $[C_{17}H_{16}]^+$-based cells and the high polarizability appears only due to the strong vibronic coupling occurring in such cells.

6. Concluding remarks

The above analysis based on the use of both semiclassical and quantum-mechanical vibronic approaches has demonstrated that the failure of the strong *U* limit is not necessary an insurmountable obstacle for the use of bi-dimers as efficient cells in QCA devices. We have shown that the occurrence of strong interaction between the excess electrons and the molecular PKS-type vibrations suggests a way to simultaneously solve the two main tasks related to the proper functioning of molecular cell in QCA, namely, to 1) to attain the charge distribution in which the electronic pair is predominantly localized in the two diagonal positions, while the sides of the cell remain unpopulated thus ensuring bi-stability and high polarizability of the cell, and 2) to make the two types of cells arrangement equivalent from the point of view of the response of the working cell to the electrostatic field induced by the driver-cell. These abilities of strong vibronic coupling called "vibronic recovering of functionality of quantum cellular automata…" in the title of this article are the results of the fact that vibronic coupling acts as interaction, which substitutes intracell Coulomb repulsion in creating the barrier between the two diagonal charge configurations. This suggests prospects to considerably expand class of possible

candidates for the role of molecular cells suitable for creating QCA devices. The general conclusions are illustrated by the *ab inito* based consideration of the two MV polycyclic derivatives of norbornadiene C_7H_8 ($[C_{12}H_{12}]^+$ and $[C_{17}H_{16}]^+$) with two C=C chromophores incorporated in the rigid polycyclic frame for which the vibronic recovery was shown to manifest itself in the shape of the cell-cell response function.

Acknowledgment

The work was in part (analysis of bidimeric cells based on the results of quantum-chemical calculations of mixed valence bridged norbornylogous compounds) performed with financial support from RSF (A.P., D.K., S.A., project No. 20-13-00374) and in part (parametric modeling of bidimeric cells with violated limit of strong Coulomb repulsion) with financial support from the Ministry of Science and Higher Education of RF (A.P., D.K., S.A., state assignment no AAAA-A19-119092390079-8). Financial support from the Spanish MICIN grant (PID2020-117177GB-I00) is gratefully acknowledged (J. M. C.).

AUTHOR DECLARATIONS

Conflict of Interest: the authors have no conflicts to disclose.

DATA AVAILABILITY

The data that support the findings of this study are available from the corresponding author upon reasonable request.

References

1. C. S. Lent, Bypassing the transistor paradigm, *Science* **2000**, *288*, 1597−1599.
2. M. Lieberman, S. Chellamma, B. Varughese, Y. Wang, C. Lent, G. H. Bernstein, G. Snider, F. C. Peiris, Quantum-dot cellular automata at a molecular scale, *Ann. N.Y. Acad. Sci*. **2002**, *960*, 225–239.
3. C. S. Lent, B. Isaksen, M. Lieberman, Molecular quantum-dot cellular automata, *J. Am. Chem. Soc*. **2003**, *125*, 1056−1063.
4. Y. Lu, C. S. Lent, Theoretical study of molecular quantum dot cellular automata. *J. Comput. Electron*. **2005**, *4*, 115−118.
5. Y. Lu, C. S. Lent, A metric for characterizing the bistability of molecular quantum-dot cellular automata. *Nanotechnology* **2008**, *19*, 155703.
6. Y. Lu, R. Quardokus, C. S. Lent, F. Justaud, C. Lapinte, S. A. Kandel, Charge localization in isolated mixed-valence complexes: an STM and theoretical study. *J. Am. Chem. Soc*. **2010**, *132*, 13519–13524.
7. Y. Lu, C. S. Lent, Field-induced electron localization: Molecular quantum-dot cellular automata and the relevance of Robin–Day classification, *Chem. Phys. Lett*. **2015**, 633, 52–57.

8. Y. Ardesi, A. Pulimeno, M. Graziano, F. Riente, G. Piccinini, Effectiveness of Molecules for Quantum Cellular Automata as Computing Devices, *J. Low Power Electron. Appl*. **2018**, 8, 24-43.

9. C. S. Lent, P. D. Tougaw, W. Porod, G. H. Bernstein, Quantum cellular automata, *Nanotechnology* **1993**, *4*, 49 −57.

10. C. S. Lent, P. D. Tougaw, W. Porod, Bistable saturation in coupled quantum dots for quantum cellular automata, *Appl. Phys. Lett*. **1993**, *62*, 714-716.

11. C. S. Lent, P. D. Tougaw, Lines of interacting quantum- dot cells: A binary wire, *J. Appl. Phys*. **1993**, *74*, 6227-6233.

12. P. D. Tougaw, C. S. Lent, Logical devices implemented using quantum cellular automata, *J. Appl. Phys*. **1994**, *75***,** 1818-1825.

13. C. S. Lent, P. D. Tougaw, A device architecture for computing with quantum dots. *Proc. IEEE,* **1997**, *85*, 541 - 557.

14. W. Porod, C. S. Lent, G. H. Bernstein, A. O. Orlov, I. Amlani, G. L. Snider, J. L. Merz, Quantum-dot cellular automata: computing with coupled quantum dots, *Int. J. Electronics,* **1999**, *86*, 549 - 590.

15. T. Ito, T. Hamaguchi, H. Nagino, T. Yamaguchi, J. Washington, C. P. Kubiak, Effects of rapid intramolecular electron transfer on vibrational spectra. *Science* **1997**, *277*, 660–663.

16. V. C. Lau, L. A. Berben, J. R. Long, $[(Cyclen)_4Ru_4(pz)_4]^{9+}$: A Creutz-Taube Square, *J. Am. Chem. Soc*. **2002**, *124*, 9042-9043.

17. H. Qi, S. Sharma, Z. H. Li, G. L. Snider, A. O. Orlov, C. S. Lent, and T. P. Fehlner, Molecular quantum cellular automata cells. electric field driven switching of a silicon surface bound array of vertically oriented two-dot molecular quantum cellular automata. *J. Am. Chem. Soc*. **2003**, 125, 15250-15259.

18. J. Jiao, G. J. Long, F. Grandjean, A. M. Beatty, T. P. Fehlner, Building blocks for the molecular expression of quantum cellular automata. isolation and characterization of a covalently bonded square array of two ferrocenium and two ferrocene complexes. *J. Am. Chem. Soc.* **2003**, *125*, 7522−7523.

19. J. Jiao, G. J. Long, L. Rebbouh, F. Grandjean, A. M. Beatty, T. P. Fehlner, Properties of a mixed-valence $(Fe^{II})_2(Fe^{III})_2$ square cell for utilization in the quantum cellular automata paradigm for molecular electronics, *J. Am. Chem. Soc*. **2005**, *127*, 17819−17831.

20. Y. Zhao, D. Guo, Y. Liu, C. He, C. Duan, A mixed-valence $(Fe^{II})_2(Fe^{III})_2$ square for molecular expression of quantum cellular automata, *Chem. Commun*. **2008**, 5725−5727.

21. V. N. Nemykin, G. T. Rohde, C. D. Barrett, R. G. Hadt, C. Bizzarri, P. Galloni, B. Floris, I. Nowik, R. H. Herber, A. G. Marrani, R. Zanoni, N. M. Loim, Electron-transfer processes in metal-free

tetraferrocenylporphyrin. understanding internal interactions to access mixed valence states potentially useful for quantum cellular automata, *J. Am. Chem. Soc*. **2009**, *131*, 14969−14978.

22. A. Burgun, F. Gendron, P. A. Schauer, B. W. Skelton, P. J. Low, K. Costuas, J.-F. Halet, M. I. Bruce, C. Lapinte, Straightforward access to tetrametallic complexes with a square array by oxidative dimerization of organometallic wires, *Organometallics* **2013**, *32*, 5015−5025.
23. B. Schneider, S. Demeshko, S. Neudeck, S. Dechert, F. Meyer, Mixed-spin [2 × 2] Fe_4 grid complex optimized for quantum cellular automata, *Inorg. Chem*. **2013**, *52*, 13230−13237.
24. J. A. Christie, R. P. Forrest, S. A. Corcelli, N. A. Wasio, R. C. Quardokus, R. Brown, S. A. Kandel, Y. Lu, C. S. Lent, K. W. Henderson, Synthesis of a neutral mixed-valence diferrocenyl carborane for molecular quantum-dot cellular automata applications*, Angew. Chem.* **2015**, 127, 15668–15671.
25. X. Wang, L. Yu, V. S. S. Inakollu, X. Pan, J. Ma, H. Yu, Molecular quantum-dot cellular automata based on diboryl radical anions, *J. Phys. Chem. C* **2018**,*122*, 2454–2460.
26. R. Makhoul, P. Hamon, T. Roisnel, J.-R. Hamon, C. Lapinte, A tetrairon dication featuring tetraethynylbenzene bridging ligand: a molecular prototype of quantum dot cellular automata, *Chem. Eur. J.,* 2020, *26*, 8368 – 8371.
27. T. Groizard, S. Kahlal, J.-F. Halet, Zwitterionic Mixed-Valence Species for the Design of Neutral Clocked Molecular Quantum-Dot Cellular Automata, *Inorg. Chem*. **2020**, 59, 15772–15779.
28. S. B. Braun-Sand, O. Wiest, Theoretical studies of mixed valence transition metal complexes for molecular computing. *J. Phys. Chem. A* **2003**, *107*, 285−291.
29. S. B. Braun-Sand, O. Wiest, Biasing mixed-valence transition metal complexes in search of bistable complexes for molecular computing, *J. Phys. Chem. B* **2003**, *107*, 9624−9628.
30. R. Wang, A. Pulimeno, M. R. Roch, G. Turvani, G. Piccinini, M. Graziano, Effect of a Clock System on Bis-Ferrocene Molecular QCA. *IEEE Trans. Nanotechnol*. **2016**, *15*, 574–582.
31. Y. H. Lu, M. Liu, C. Lent, Molecular quantum-dot cellular automata: From molecular structure to circuit dynamics. *J. Appl. Phys*. **2007**, *102*, 034311.
32. B. Tsukerblat, A. Palii, J. M. Clemente-Juan, Self-trapping of charge polarized states in four-dot molecular quantum cellular automata: bi-electronic tetrameric mixed valence species, *Pure Appl. Chem.* **2015,** *87*, 271–282.
33. B. Tsukerblat, A. Palii, J. M. Clemente-Juan, E. Coronado, Mixed-valence molecular four-dot unit for quantum cellular automata: vibronic self-trapping and cell-cell response, *J. Chem. Physics,* **2015,** *143*, 134307-15.
34. A. Palii, B. Tsukerblat, J. M. Clemente-Juan, E. Coronado, Spin-switching in molecular quantum cellular automata based on mixed-valence tetrameric units, *J. Phys. Chem.*, **2016,** *120*, 16994−17005.
35. A. Palii, B. Tsukerblat, Tuning of quantum entanglement in molecular quantum cellular automata based on mixedvalence tetrameric units, *Dalton Trans*. **2016**, *45*, 16661–16672.

36. J. M. Clemente-Juan, A. Palii, E. Coronado, B. Tsukerblat, Mixed-Valence Molecular Unit for Quantum Cellular Automata: Beyond the Born-Oppenheimer Paradigm through the Symmetry Assisted Vibronic Approach, *J. Chem. Theory Comp.* **2016,** *12*, 3545−3560.

37. A. Palii, A. Rybakov, S. Aldoshin, B. Tsukerblat, Semiclassical versus quantum mechanical vibronic approach in the analysis of the functional characteristics of molecular quantum cellular automata, *Phys. Chem. Chem. Phys.*, **2019**, *21,* 16751-16761.

38. A. Palii, S. Zilberg, A. Rybakov, B. Tsukerblat, Double-dimeric versus tetrameric cells for quantum cellular automata: a semiempirical approach to evaluation of cell−cell responses combined with quantum-chemical modeling of molecular structures, *J. Phys. Chem. C,* **2019**, *123*, 22614−22623.

39. A. Palii, S. Aldoshin, S. Zilberg, B. Tsukerblat, Parametric two-mode vibronic model of a dimeric mixed valence cell for molecular quantum cellular automata and computational ab-initio verification, *Phys.Chem.Chem.Phys*. **2020**, *22*, 25982-25999.

40. A. Palii, J. M. Clemente-Juan, S. Aldoshin, D. Korchagin, A. Rybakov, S. Zilberg, B. Tsukerblat Mixed-Valence Magnetic Molecular Cell for Quantum Cellular Automata: Prospects of Designing Multifunctional Devices through Exploration of Double Exchange, *J. Phys. Chem. C* **2020**, *124*, 25602−25614.

41. B. Tsukerblat, A. Palii, S. Aldoshin, Molecule Based Materials for Quantum Cellular Automata: A Short Overview and Challenging Problems, *Isr. J. Chem.* **2020**, *60*, 527–543.

42. A. Palii, J. M. Clemente-Juan, A. Rybakov, S. Aldoshin, B. Tsukerblat, Exploration of the double exchange in quantum cellular automata: proposal for a new class of cells, *Chem. Comm.* **2020**, *56*, 10682–10685.

43. A. Palii, S. Aldoshin, B. Tsukerblat, Towards the design of molecular cells for quantum cellular automata: critical reconsideration of the parameter regime for achieving functionality, *Dalton Trans.* **2022**, *51*, 286–302.

44. S. S. Pidaparthia, C. S. Lent, Molecular reorganization energy in quantum-dot cellular automata switching, *J. Appl. Phys*. **2022**, *131*, 044502.

45. S. B. Piepho, E. R. Krausz, P. N. Schatz, Vibronic coupling model for calculation of mixed valence absorption profiles, *J. Am. Chem. Soc*. **1978**, *100*, 2996–3005.

46. K. Prassides, P.N. Schatz, Vibronic coupling model for mixed valence compounds: extension to the multimode case, *J. Phys. Chem*. **1989**, *93*, 83–89.

47. K.Y. Wong, Charge-transfer-induced IR absorptions in mixed valence compounds, *Inorg. Chem*. **1984**, *23*, 1285–1290.

48. K.Y. Wong, P.N. Schatz, A dynamic model for mixed-valence compounds, *Prog. Inorg. Chem*. **1981**, *28*, 369–449.

49. S. B. Piepho, Vibronic coupling model for the calculation of mixed-valence line shapes: the interdependence of vibronic and MO effects, *J. Am. Chem. Soc*. **1988**, *110*, 6319–6326.

50. S. B. Piepho, Vibronic coupling model for the calculation of mixed-valence line shapes: a new look at the Creutz-Taube ion, *J. Am. Chem. Soc*. **1990**, *112*, 4197–4206.

51. S. A. Borshch, I. N. Kotov, I. B. Bersuker, Electron delocalization in trinuclear mixed-valence clusters, *Chem. Phys. Lett*. **1982**, *89*, 381–384.

52. J. P. Launay, F. Babonneau, Semiclassical model of a trinuclear mixed valence system, *Chem. Phys.* **1982**, *67*, 295–300.

53. S. A. Borshch, L. F. Chibotaru, Electron delocalization in trinuclear iron-sulfur clusters from Desulfovibrio Gigas, *Chem. Phys*. **1989**, 135, 375–380.

54. S. A. Borshch, E. L. Bominaar, G. Blondin, J. J. Girerd, Double exchange and vibronic coupling in mixed valence systems. Origin of the broken-symmetry ground state of $[Fe_3S_4]^0$ cores in proteins and models, *J. Am. Chem. Soc*. **1993**, *115*, 5155–5168.

55. A. J. Marks, K. Prassides, Vibronic effects in a model four center, one-electron mixed-valence system, *New J. Chem*. **1993**, *17*, 59–65.

56. A. J. Marks, K. Prassides, Exchange and vibronic interactions in a tetrahedral, five-electron mixed-valence cluster, *J. Chem. Phys*. **1993**, *98*, 4805–4813.

57. S. I. Boldyrev, V. Y. Gamurar, B. S. Tsukerblat, A. V. Palii, Vibronic interaction in multielectronic mixed-valence trimeric clusters, *Mol. Phys*. **1994**, *81*, 621–654.

58. J. M. Clemente-Juan, A. Palii, B. Tsukerblat, E. Coronado, VIBPACK: a package to treat multidimensional electron-vibrational molecular problems with application to magnetic and optical properties*, J. Comput. Chem*. **2018**, *39*, 1815–1827.

59. A. Palii, S. Aldoshin, B. Tsukerblat, J. M. Clemente-Juan, E. Coronado, Vibronic model for intercommunication of localized spins via itinerant electron, *J. Phys. Chem. C* **2019**, *123*, 5746–5760.

60. A. Palii, B. Tsukerblat, Pair-delocalization in trigonal mixed-valence clusters: new insight into the vibronic origin of broken-symmetry ground states, *PhysChemChemPhys*, **2019**, *21*, 11122–11131.

61. C. Bosch-Serrano, J. M. Clemente-Juan, E. Coronado, A. Gaita-Ariño, A. Palii, B. Tsukerblat, Electric field control of the spin state in mixed-valence magnetic molecules, *Chem. Phys. Chem.* **2012**, *13*, 2662–2665.

62. C. Bosch-Serrano, J. M. Clemente-Juan, E. Coronado, A. Gaita-Ariño, A. Palii, B. Tsukerblat, Molecular analog of multiferroics: electric and magnetic field effects in many-electron mixed-valence dimers, *Phys. Rev. B* **2012**, *86*, 024432.

63. A. Palii, B. Tsukerblat, J. M. Clemente-Juan, E. Coronado, Coherent manipulation of polarization in mixed-valence compounds by electric pulse via Landau-Zener transitions, *J. Phys. Chem. C* **2012**, *116*, 4999–5008.

64. A. Palii, J. M. Clemente-Juan, B. Tsukerblat, E. Coronado, Electric field control of the optical properties in magnetic mixed valence molecules, *Chem. Sci*. **2014**, *5*, 3598–3602.

65. H. Qi, A. Gupta, B. C. Noll, G. L. Snider, Y. Lu, C. Lent, T. P. Fehlner, Dependence of Field Switched Ordered Arrays of Dinuclear Mixed-Valence Complexes on the Distance between the Redox Centers and the Size of the Counterions, *J. Am. Chem. Soc*. **2005**, 127, 15218-15227.

66. S. Zilberg, Y. Stekolshik, A. Palii, B. Tsukerblat, Controllable Electron Transfer in Mixed-Valence Bridged Norbornylogous Compounds: Ab Initio Calculation Combined with a Parametric Model and Through-Bond and Through-Space Interpretation, *J. Phys. Chem. A* **2022**, *126*, 19, 2855–2878.

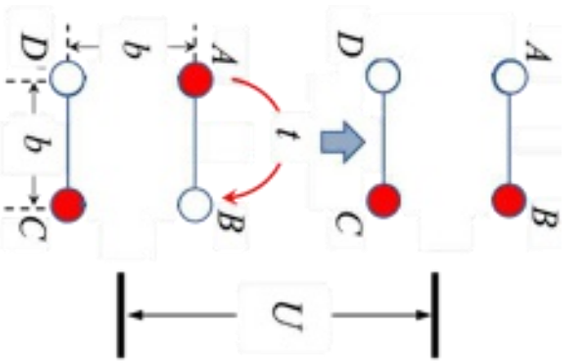

Figure 1

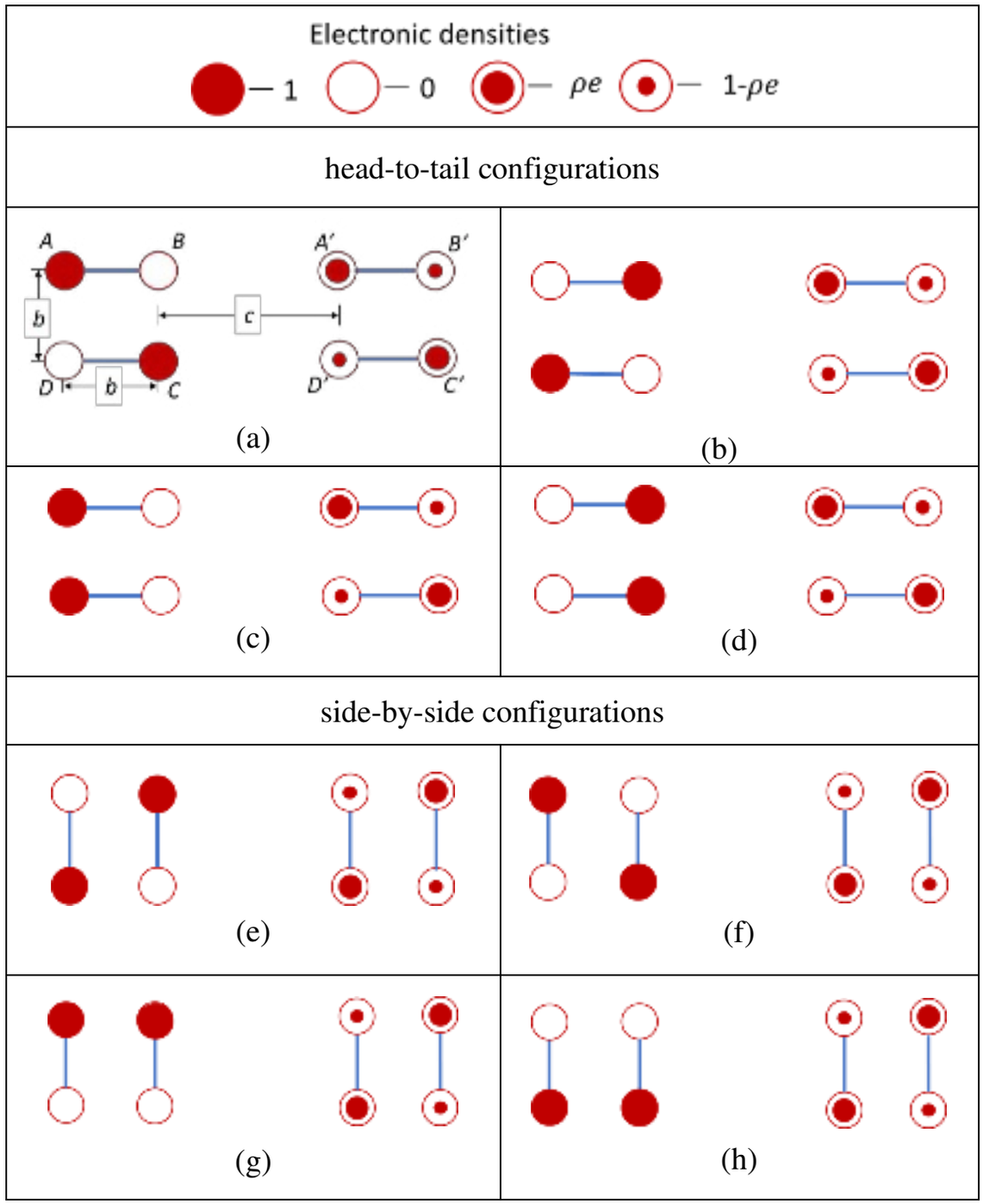

Figure 2

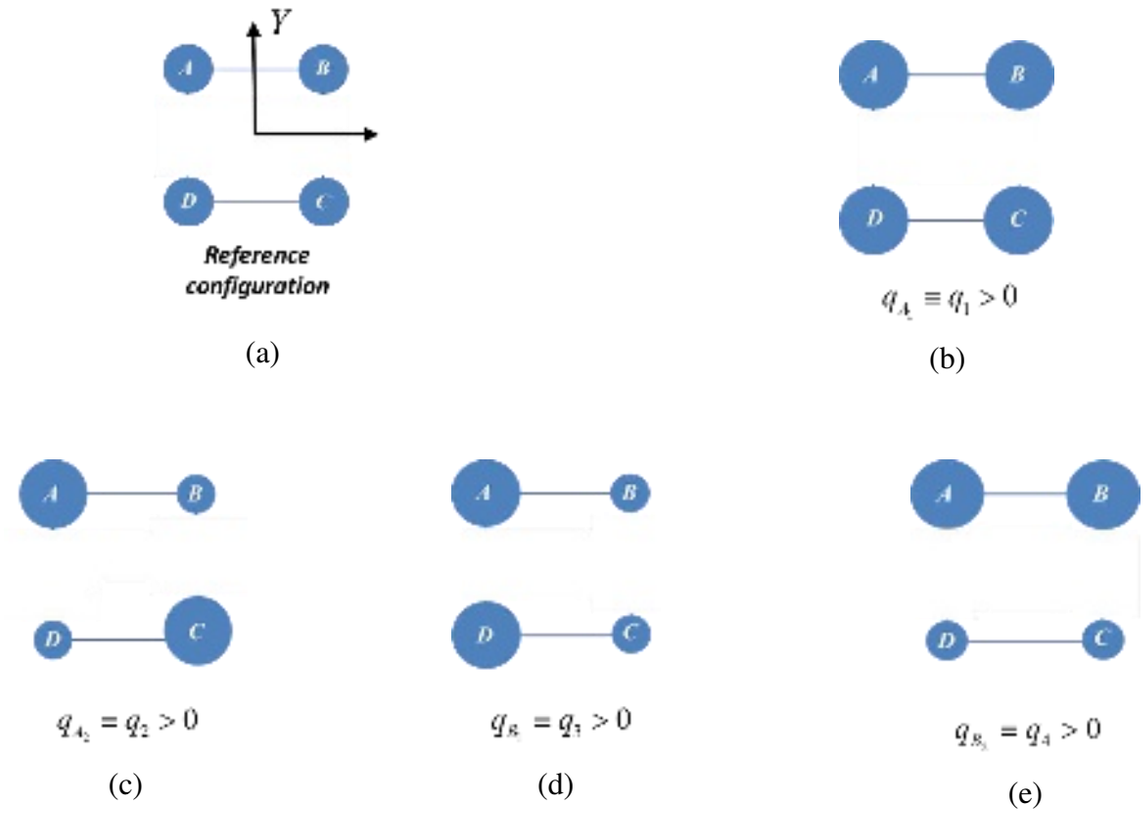

Fig.3

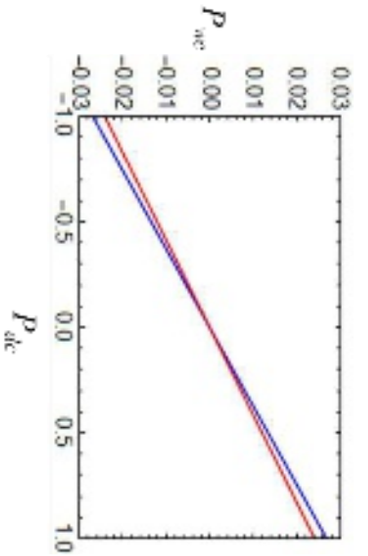

Fig. 4

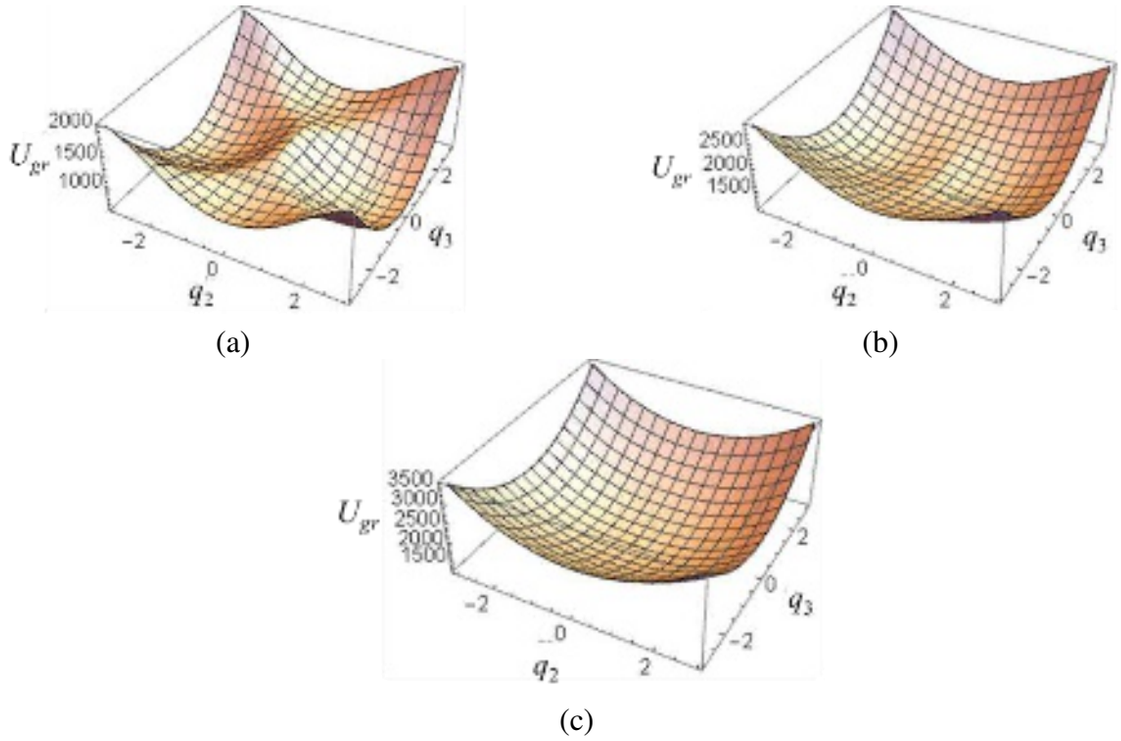

(a) (b)

(c)

Fig. 5.

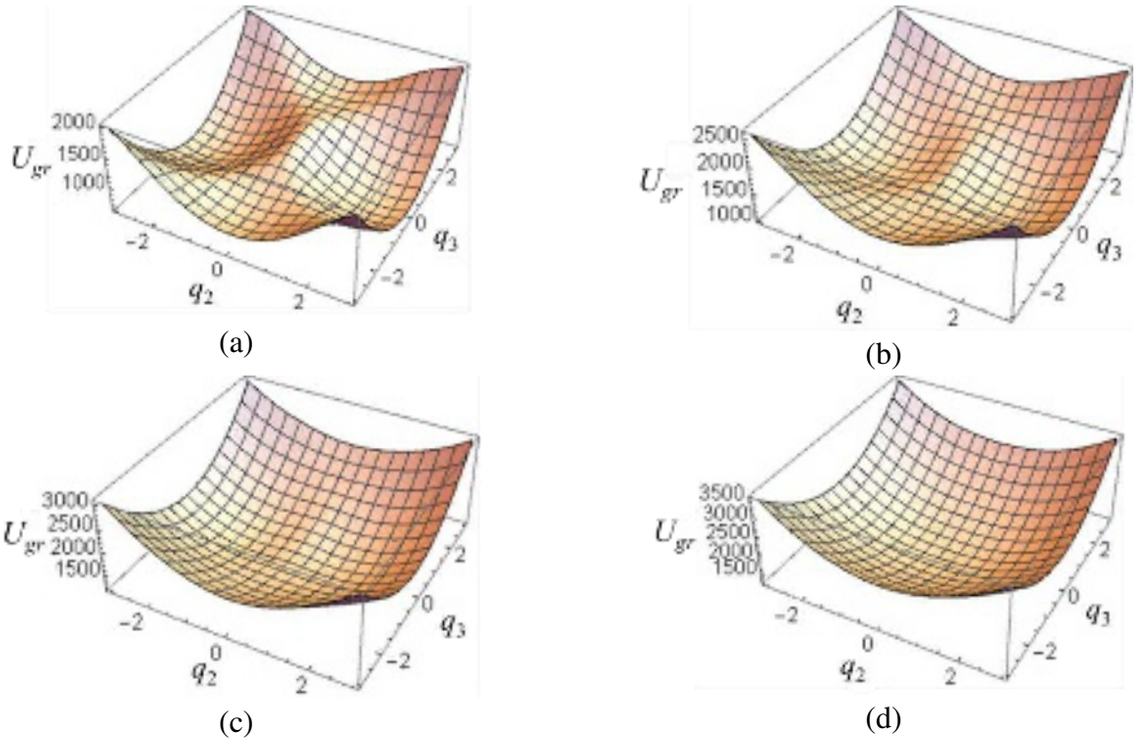

.

Fig. 6

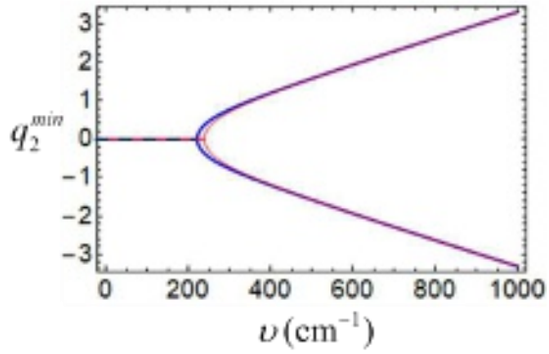

(a)

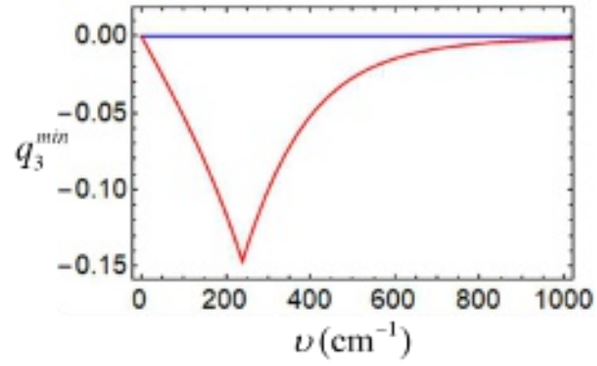

(b)

Fig. 7.

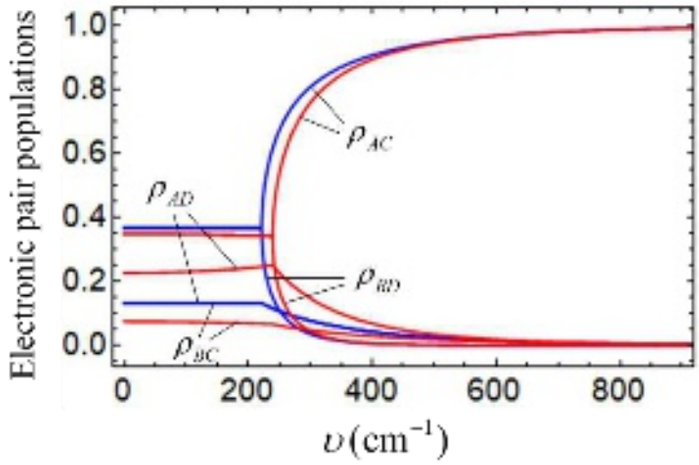

Fig. 8

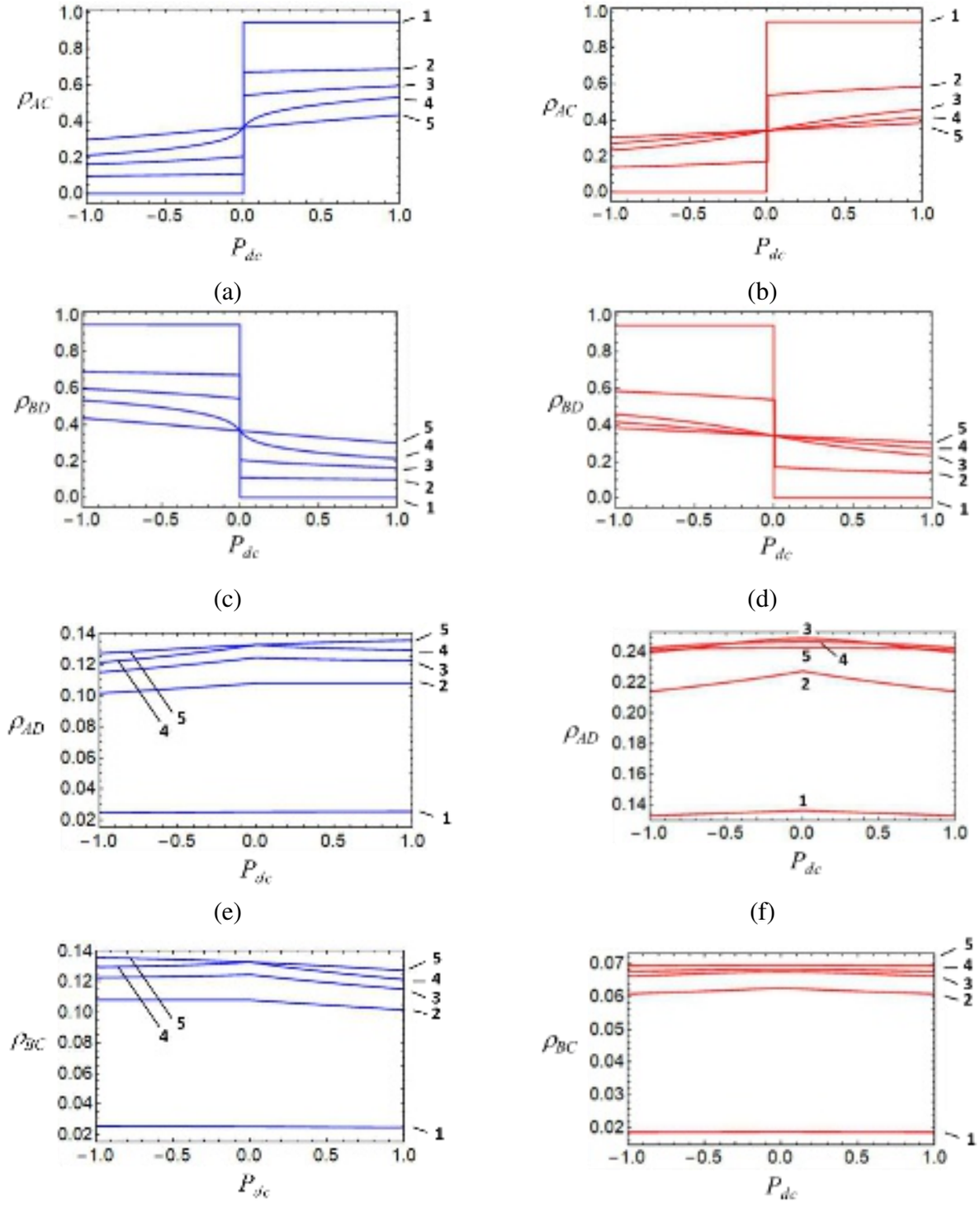

Fig. 9.

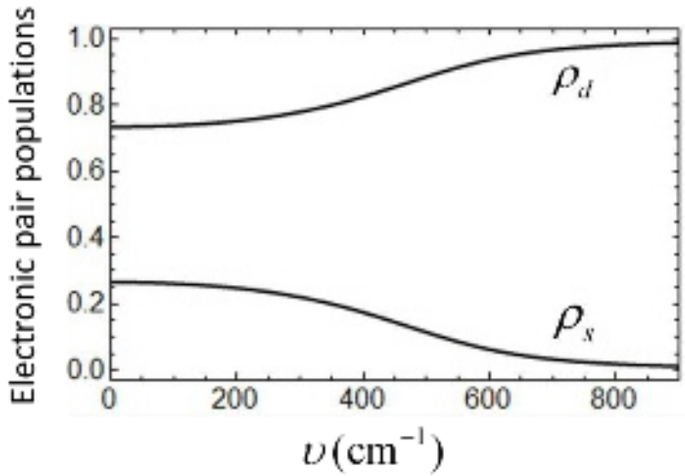

Fig. 10

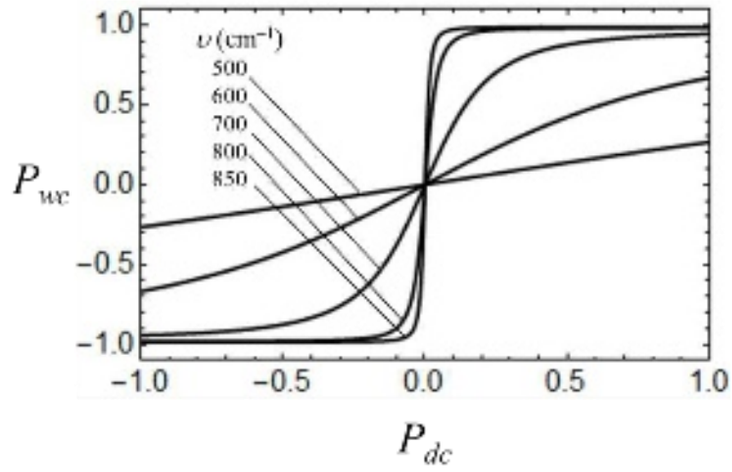

Fig. 11

Fig. 12

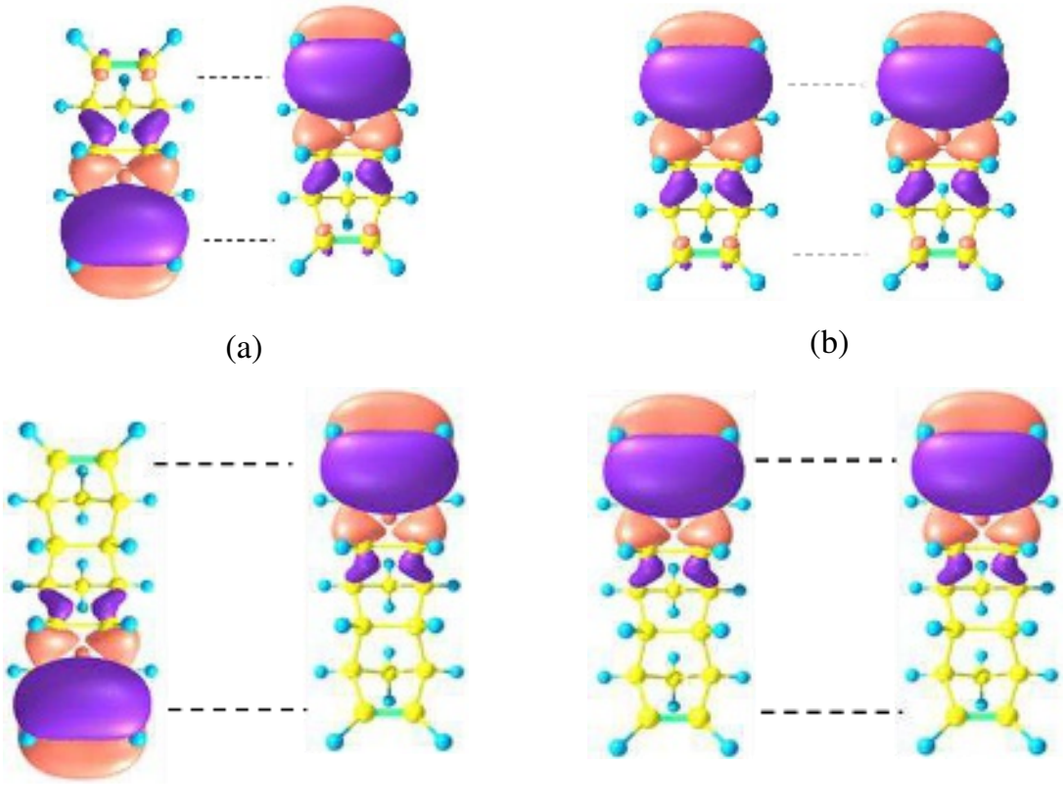

Fig. 13.

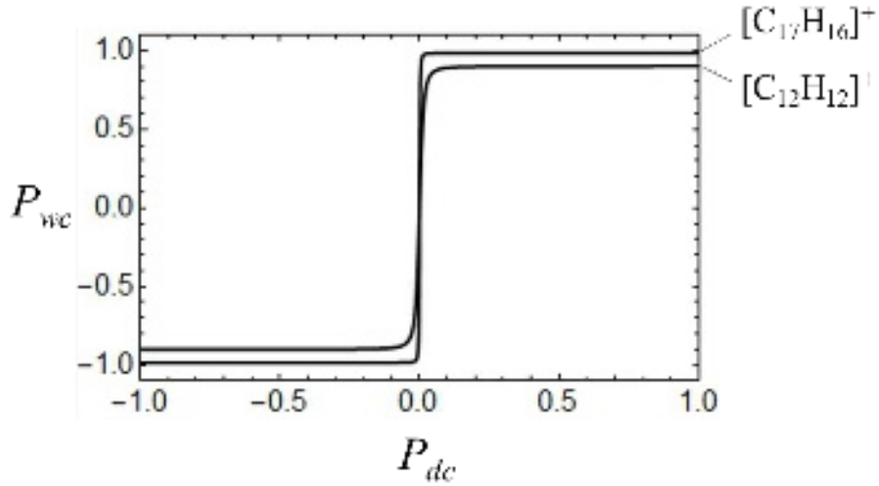

Fig. 14.